

POLITECNICO DI TORINO

Master degree in Energy and Nuclear Engineering

Master Thesis

**OPTIMIZATION OF A SIMULTANEOUS  
COMPRESSION/DISSOLUTION PROCESS OF  
CARBON DIOXIDE IN WATER**



**Supervisors**

Prof. Dr.-Ing. Massimo Santarelli  
Prof. Dr.-Ing. Dimosthenis Trimis

**Candidate**

Antonio Zanghi

Luglio 2018



I declare that this thesis has been composed solely by myself and that it has not been submitted, in whole or in part, in any previous application for a degree. Except where states otherwise by reference or acknowledgment, the work presented is entirely my



## **Abstract**

The effects of temperature rising due to the increasing amount of greenhouse gases are already easily visible. The most immediate consequences is the increase of unusual atmospheric events like tropical hurricanes and precipitations which lead to undesirable results as sea levels risings, desertification and moving of earth climatic area. The target announced by the Conference of Paris in 2015 sets a goal to limit the increase of temperature up to 1.5°C in respect to the pre-industrial age. The achievement of this goal can be considered the biggest challenge of this century and requires a huge effort from all the international community in order to face a strong decarbonisation process in most of the society sections.

Already, big effort has been carried out in this direction, but much more investments are needed in the next decades in order to increase the amount of energy produced by renewable fuels. The increase of fluctuating renewable energy generation will lead to stability problems in the electric grid. This results to pay bigger attention on solutions on how to store the renewable energy surplus. The power to chemicals technologies appears as a promising solution for a long-term electricity storage. It is able to deal with different applications in terms of release time and amount of stored energy. The simultaneous compression/dissolution process of CO<sub>2</sub> and water investigated in this work is part of the European project CELBICON, which aims to create added value chemicals with high global efficiency.

This technology promise a theoretical energy saving of about 40 % compared to the traditional separate gas and water compression with subsequent dissolution.

This energy saving is given by the combination of high isothermal behaviour of the process because of the big heat capacity of the sprayed water and by the reduced gaseous mole to compress because of dissolution occurrence.

Experiments are performed varying nozzles and the compression speed in order to understand how the process evolves for different spray pattern and different dissolution time.

The obtained results show near values to the theoretical target, this allows to take into account this technology for further applications.



## TABLE OF CONTENTS

<b>1</b>	<b>INTRODUCTION .....</b>	<b>17</b>
<b>2</b>	<b>THEORY AND LITERARY REVIEW .....</b>	<b>23</b>
2.1	THEORY .....	23
2.1.1	<i>CO<sub>2</sub> Dissolution .....</i>	<i>23</i>
2.1.2	<i>Atomization and Spray .....</i>	<i>24</i>
2.1.3	<i>Water gas Interface .....</i>	<i>31</i>
2.1.4	<i>Thermodynamics of compression .....</i>	<i>34</i>
2.2	LITERATURE REVIEW .....	35
<b>3</b>	<b>EXPERIMENTAL SETUP AND PROCEDURE .....</b>	<b>39</b>
3.1	EXPERIMENTAL SETUP.....	39
3.2	EXPERIMENTAL PROCEDURE .....	47
3.2.1	<i>Water amount calculation.....</i>	<i>47</i>
3.2.2	<i>Piston speed evaluation.....</i>	<i>48</i>
3.2.3	<i>Nozzle selection and flowrate evaluation.....</i>	<i>52</i>
3.2.4	<i>Experiments implementation.....</i>	<i>54</i>
3.3	DATA GATHERING AND FILTERING METHOD .....	56
<b>4</b>	<b>RESULTS .....</b>	<b>66</b>
4.1	OUTCOMES FOR DIFFERENT NOZZLE AND SPEED PROFILE .....	66
4.2	REFERENCE CASES .....	69
4.3	WORK ESTIMATION .....	72
4.4	CELBICON CONFIGURATION .....	74
<b>5</b>	<b>CONCLUSIONS .....</b>	<b>79</b>
<b>6</b>	<b>REFERENCES .....</b>	<b>81</b>
<b>7</b>	<b>APPENDIX.....</b>	<b>84</b>

## List of tables

TABLE 1 DROPLET DIAMETER FOR A GIVEN PERCENTAGE OF DISSOLUTION DURING THE TRANSITORY OF 1BAR PRESSURE INCREASE	33
TABLE 2 HYDRAULIC UNIT, MAIN SPECIFICATIONS.....	41
TABLE 3 PISTON COMPRESSOR SPECIFICATIONS .....	41
TABLE 4 PUMP AND PRESSURE REGULATOR SPECIFICATIONS.....	43
TABLE 5 NOZZLES TECHNICAL SPECIFICATIONS .....	46
TABLE 6 PARAMETERS INVOLVED IN THE WATER AMOUNT CALCULATION .....	48
TABLE 7 NOZZLES OPERATIONAL PARAMETERS .....	53
TABLE 8 RESUME OF EXPERIMENT PARAMETERS.....	66
TABLE 9 PARAMETER FOR REFERENCE CASES EVALUATION.....	70
TABLE 11 DISSOLUTION EFFICIENCY .....	74
TABLE 12 CELBICON CONFIGURATION - MAIN PARAMETERS .....	75

## LIST OF FIGURES

FIGURE 1 TEMPERATURE INCREASE FOR DIFFERENT SCENARIO- POTSDAM INSTITUTE FOR CLIMATE IMPACT RESEARCH [1] .....	17
FIGURE 2 PERCENTAGE OF GREENHOUSE GAS EMISSION BY ECONOMIC SECTOR AT THE LEFT AND COMPOSITION OF GREENHOUSE GAS AT THE RIGHT [2] .....	18
FIGURE 3 ENERGY STORAGE SYSTEMS FOR DIFFERENT APPLICATIONS [3] .....	19
FIGURE 4 CELBICON PROJECT ILLUSTRATION [3] .....	20
FIGURE 5 PISTON COMPRESSOR WITH INTEGRATED NOZZLE FOR SIMULTANEOUS COMPRESSION/DISSOLUTION PROCESS .....	21
FIGURE 6 MUTUAL ATTRACTION OF LIQUID MOLECULES AT INTERFACE [7] .....	25
FIGURE 7 VARIATION OF SPHERE RADIUS [7] .....	26
FIGURE 8 AERODYNAMIC FORCES AT THE INTERFACE LIQUID/GAS .....	29
FIGURE 10 LIQUID INJECTION COMPRESSOR INVENTOR WILFRED J ROULEAU US PATENT [17] .....	36
FIGURE 11 COMPONENTS DIAGRAM OF THE EXPERIMENTAL SETUP .....	39
FIGURE 11 SPRAY PATTERN FOR HOLLOW-CONE AT THE LEFT AND FULL-CONE AT THE RIGHT [21] .....	45
FIGURE 12 CASE A AND CASE B, SPEED SLOPE COMPARISON .....	49
FIGURE 13 FLOWRATE EVALUATION FOR THE TWO NOZZLES .....	53
FIGURE 14 MEASUREMENT NOISE .....	56
FIGURE 15 EXPONENTIAL APPROXIMATION OF EXPERIMENTAL DATA FOR CASE B NOZZLE 1 .....	57
FIGURE 16 PRESSURE SENSOR ERROR, ZOOM AT BEGINNING OF COMPRESSION .....	59
FIGURE 17 COMPARISON OF DIFFERENT REDUCTION NOISE METHOD VARYING THE SPAN NUMBER .....	60
FIGURE 18 CASE A NOZZLE 1 APPROXIMATION OF THE FIRST EXPERIMENT .....	62
FIGURE 19 AVERAGE CURVE WITH RAW DATA OF CASE A NOZZLE 1 .....	64
FIGURE 20 RSD OVER 5 EXPERIMENTS OF CASE A NOZZLE 1 .....	65
FIGURE 21 CASE A AND CASE B COMPARISON, INJECTION NOZZLE 1 AND NOZZLE 2 .....	68
FIGURE 22 A AND B CASE COMPARISON WITH REFERENCE CASES .....	71
FIGURE 23 WORKS EVALUATION (9BARG) EFFICIENCY ESTIMATION .....	73
FIGURE 24 CELBICON CONDITIONS - SPEED PROFILE COMPARISON .....	76
FIGURE 25 CELCIBON CONFIGURATION - CASE A AND CASE B COMPARISON WITH REFERENCE CASES .....	77
FIGURE 26 WORKS EVALUATION OF THE CELBICON CASE .....	78

## LIST OF PICTURES

PICTURE 1 CO <sub>2</sub> CYLINDER AT THE LEFT, HYDRAULIC SYSTEM(A) AND COMPRESSION/DISSOLUTION UNIT (B IN THE CENTER), AND INJECTION SYSTEM (C) AT THE RIGHT.....	40
PICTURE 2 HYDRAULIC UNIT: OIL PUMP AT THE RIGHT AND OIL FAN COOLER AT THE LEFT.....	40
PICTURE 3 PISTON COMPRESSOR.....	42
PICTURE 4 INJECTION SYSTEM, WATER PUMP FILTER AND WATER TANK.....	43
PICTURE 6 INJECTION SYSTEM, RECIRCULATION BRANCH AND OVERPRESSURE VALVE.....	44
PICTURE 7 INJECTION, CO <sub>2</sub> AND EXITING LINE LOCATED ON THE TOP OF THE PISTON.....	45
PICTURE 8 NOZZLE IMAGE AND TECHNICAL DRAWING.....	46
PICTURE 11 LABVIEW CODE FOR COMPRESSION PHASE WITH CONSTANT SPEED.....	51
PICTURE 12 LABVIEW CODE CHANGE FOR VARIABLE SPEED.....	51
PICTURE 13 LABVIEW CONTROL WINDOW.....	55

## LIST OF ABBREVIATIONS

<i>COP 21</i>	<i>21th Conference of Paris</i>
<i>IPCC</i>	<i>Intergovernmental Panel on Climatic Change</i>
<i>PHA</i>	<i>polyhydroxyalkanoate</i>
<i>CELBICON</i>	Cost – effective CO <sub>2</sub> conversion into chemicals via combination of Capture, Electrochemical and Biochemical CONversion technologies
<i>DAC</i>	<i>direct air capture technology</i>
<i>SMD</i>	<i>Sauter Mean Diameter</i>
<i>NI – QBOX</i>	National Instrument acquisition data tool

## LIST OF SYMBOLS

<i>symbol</i>	<i>description</i>	<i>unit</i>
$C$	<i>Henry's Law constant</i>	$K$
$D$	<i>diffusion coefficient</i>	$m^2s^{-1}$
$D_s$	<i>Sauter diameter</i>	$\mu m$
$E_a$	<i>global energy of atomization</i>	$J$
$E_c$	<i>kinetic energy of atomization</i>	$J$
$E_s$	<i>surface energy of atomization</i>	$J$
$E_c$	<i>kinetic energy of atomization</i>	$J$
$F_c$	<i>capillary force</i>	$N$
$F_G$	<i>gravitational force</i>	$N$
$F_v$	<i>viscous force</i>	$N$
$Fo$	<i>dimensionless Fourier number</i>	$/$
$J$	<i>diffusion flux</i>	$mol\ m^{-2}s^{-1}$
$k = \frac{c_p}{c_v}$	<i>heat capacity ratio</i>	$/$
$k_H^0$	<i>Henry's Law constant at 25°C</i>	$mol\ kg^{-1}\ bar^{-1}$
$k_H(T)$	<i>Henry's Law constant depending on temperature</i>	$mol\ kg^{-1}\ bar^{-1}$
$L$	<i>carachteristic length</i>	$m$
$L_c$	<i>capillarity length</i>	$m$
$L_{DC}$	<i>dissipation length of capillary waves</i>	$m$
$m_{CO_2}$	<i>CO<sub>2</sub> mass</i>	$kg$
$M_{CO_2}$	<i>molar mass of CO<sub>2</sub></i>	$g\ mol^{-1}$
$n_{CO_2}^0$	<i>initial CO<sub>2</sub> moles</i>	$mol$
$Oh$	<i>Ohnesorge number</i>	$/$
$p$	<i>partial pressure of solute above the solution</i>	$bar$
$p_g$	<i>perpendicular aerodynamic force</i>	$N$

$r$	<i>droplet ray</i>	$\mu\text{m}$
$R$	<i>ideal gas constant</i>	$\text{kJ kg}^{-1} \text{K}^{-1}$
<i>stroke</i>	<i>piston stroke</i>	$\text{mm}$
$T^0$	<i>standard temperature</i>	$\text{K}$
$T_C$	<i>critical temperature</i>	$\text{K}$
$V$	<i>velocity</i>	$\text{m s}^{-1}$
$V_{\text{chamber}}$	<i>chamber volume</i>	$\text{m}^3$
$V_{\text{H}_2\text{O}}^0$	<i>injected water volume</i>	$l$
$V_{\text{CO}_2}^0$	<i>gas volume in Chamber</i>	$\text{m}^3$
$We_g$	<i>Weber number for gas</i>	/
$We_l$	<i>Weber number for liquid</i>	/
$W_{\text{isentrop}}$	<i>isentropic work of compression</i>	$J$
$W_{\text{liquid}}$	<i>liquid compression work</i>	$J$
$x$	<i>concentration</i>	$\text{mol kg}^{-1}$
$\Delta P$	<i>difference of pressure</i>	$\text{bar}$
$\Delta t_{\text{step}}$	<i>average time to increase pressure</i>	$\text{s bar}^{-1}$
$\eta_a$	<i>efficiency of atomization</i>	/
$\theta_0$	<i>initial concentration value</i>	$\text{mol kg}^{-1}$
$\theta(r, t)$	<i>concentration in function of droplet radius and time</i>	$\text{mol kg}^{-1}$
$\theta_{\text{inf}}$	<i>saturation concentration value (Henry's Law)</i>	$\text{mol kg}^{-1}$
$\mu$	<i>viscosity</i>	$\text{m}^2 \text{s}^{-1}$
$\rho_{\text{CO}_2}$	<i>CO<sub>2</sub> density</i>	$\text{kg m}^{-3}$
$\sigma$	<i>surface tension</i>	$\text{mN m}^{-1}$
$\nabla^2$	<i>Laplacian operator</i>	/



## SUMMARY

The current work begins by giving an overview of the reasons and the long term climate impacts that lead to global attention on the reduction of greenhouse emissions (CO<sub>2</sub>). The need of society to develop a Low-Carb direction justifies increasing investments and efforts in renewable sources of power and as effect in the production of added value chemical compounds as way to store energy and reduce the electric grid instability.

The central topic of this work, the compression/dissolution process, is part of a European project CELBICON, that aims to produce chemicals starting from surplus energy and atmospheric CO<sub>2</sub>. An overview of the project is presented. The theory that rules the process is investigated in order to set properly the experimental parameters. More specifically, an overall introduction is given for the atomization that determines the spray pattern. Also, the dissolution process of CO<sub>2</sub> in water is described along with the diffusion process that rules the transitory of dissolution at the gas/liquid interface and finally the thermodynamic laws that rule the compression.

A description of the experimental setup is also provided, giving attention to the most critical components, followed by a careful description of the procedure adopted for the conduction of the experiments and the selection of the parameters. In the experiments, the dissolution process is investigated for different spray pattern and different piston speed profiles of compression. To continue with, a description of the data gathering and data filtering process with deep focus on measurement errors is presented.

The results are provided with particular attention to the energy saving obtained during the compression in respect to the reference cases properly defined. The outcomes of this work allows us to understand what enhances the dissolution process and most importantly which are the compression phases in which the variation of parameters has more influence. The work concludes with a discussion on the achieved results considering the need to make further investigations using alternative spray pattern or alternative chamber geometry.



# 1 Introduction

The climate change, which effects are already visible around the world, has been largely attributed to the rise of the greenhouse gas; many effort have been done in the last decades by the international community in order to reduce the emissions developing alternatives to fossil fuels.

In Figure 1 are shown the several probable scenarios of temperature rising until 2100 analysed by the “Potsdam Institute for Climate Impact Research”, is visible that limiting the increase of temperature “under 1.5°C with respect to pre-industrial levels within 2100” and “well under 2°C” in long term (COP 21 [1]) is something that require a drastic reduction of the global emissions in the next decades.

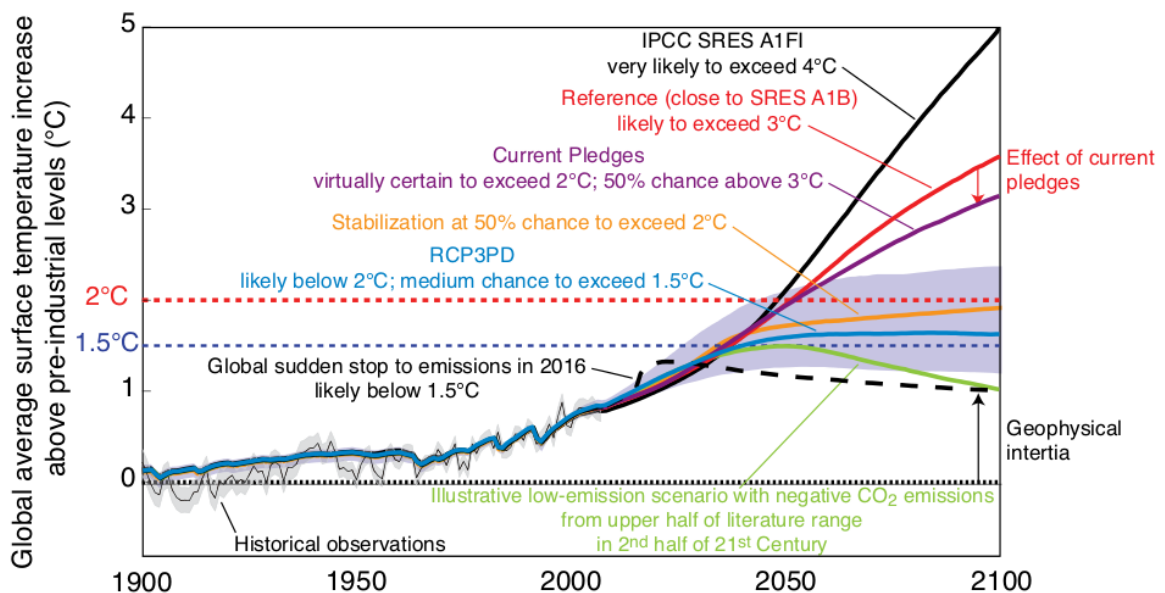


Figure 1 Temperature increase for different scenario- Potsdam Institute for Climate Impact Research [1]

According to the last report of the Intergovernmental Panel on Climatic Change (IPCC) of 2014, as visible in Figure 2 the biggest percentage of greenhouse gas emission is produced by the sector of electricity and heat production while the 65% of the global greenhouse consist in Carbon Dioxide coming from fossil fuel and industrial processes [2].

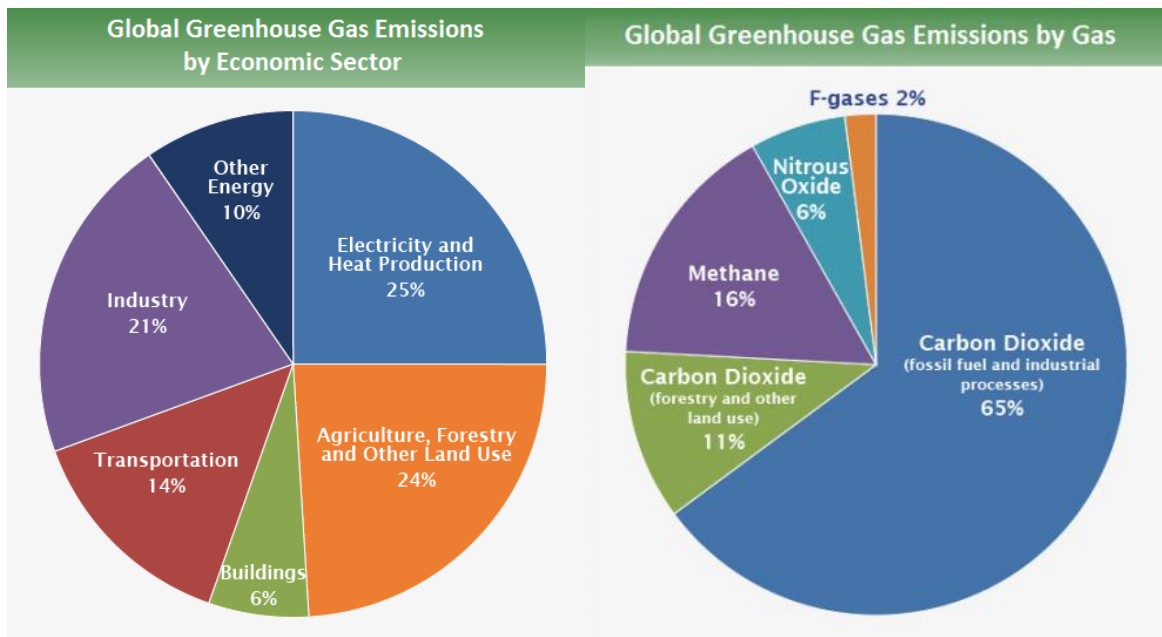


Figure 2 percentage of greenhouse gas emission by economic sector at the left and composition of greenhouse gas at the right [2]

Follows that the conversion of the actual society to a Low-Carbon alternative one will be one of the biggest challenge of this century. This conversion process must include a gradually conversion of fossil fuels based energy production to energy produced from renewable source. The Increasing production of renewable source characterized by high unpredictability will increase the instability of the energy production, for this reason several strategies are put in place from the scientific community and storage and reuse technologies appears to be fundamental in order to sustain the Low- Carb conversion process.

As is also visible in Figure 3 among all the different main technologies to store energy, the production of fuel like Hydrogen and Methane from electrolyse process appears to be the best choice in terms of amount of energy that can be stored and release time [3].

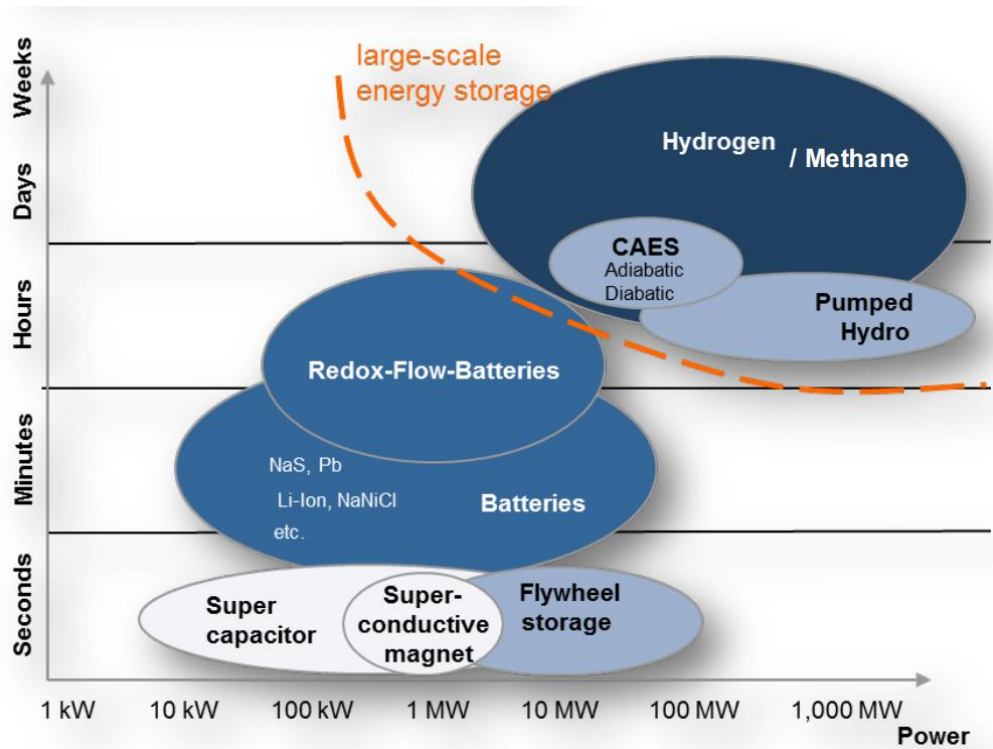


Figure 3 Energy Storage systems for different applications [3]

The aim of this kind of energy storage lies in the upgrade of lower chemical enthalpy compounds in upper ones by means of an electrolysis process. This kind of enthalpy upgrade can be performed in order to obtain fuel usually in gaseous or liquid form, but also to produce high value compounds like bioplastic as in the case of the CELBICON Project.

CELBICON is a project funded by the European commission through the program Horizon 2020, it is the acronym of "Cost-effective CO<sub>2</sub> conversion into chemicals via combination of Capture, Electrochemical and Biochemical CONversion technologies". This project aims to develop a new CO<sub>2</sub>-to chemicals approach exploiting CO<sub>2</sub> capture, electrochemical CO<sub>2</sub> conversion and fermentation in order to produce value added chemicals. As the title of the process underlines, big importance is given to the achievement of high products yields using moderate operating temperature and maintenance costs. Also, big importance is given to the overall efficiency of the process in terms of energy use reduction in order to allow a faster market penetration of the technology. A first scheme of the projects production line is provided in Figure 4 [4].

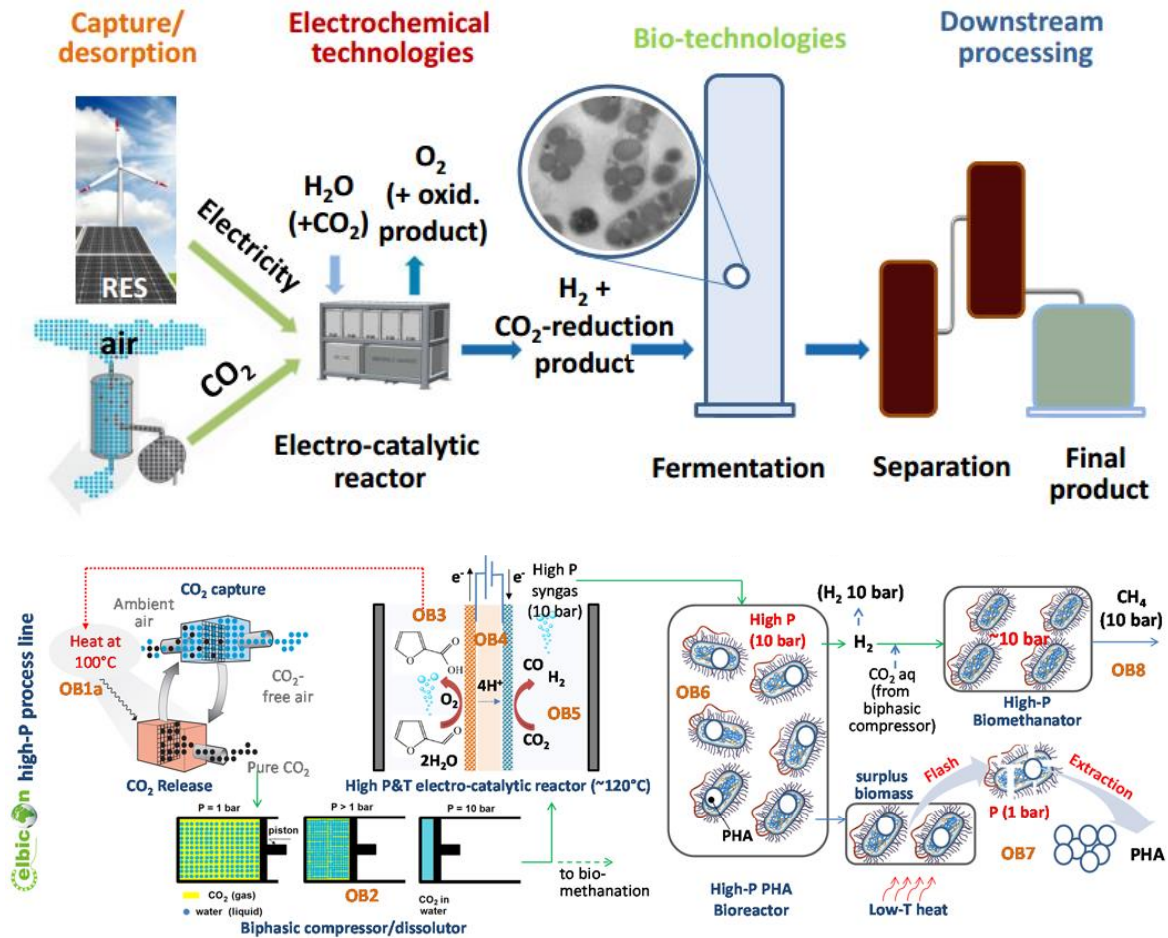


Figure 4 CELBICON project illustration [4]

As is shown in Figure 4 the CELBICON project aims to produce PHA (Polyhydroxyalkanoate) bioplastic and pressurized methane from electrochemical conversion of a flow of CO<sub>2</sub> and water simultaneously pressurized in a volumetric compressor. The goal of this process is the storage of surplus electricity from renewable fuel of power in added chemical compound like bioplastic and methane. The CO<sub>2</sub> that will feed the cathode of the electrolyser is extracted from the atmosphere using a direct air capture technology (DAC), this technology exploits the adsorption/desorption phenomenon. As is possible to observe in Figure 4 the pressure increase of the electrolyser inlet flow is provided by an innovative volumetric compressor that allows simultaneous compression of the CO<sub>2</sub>/water mixture. The conventional way to obtain the same result is to compress water and gas separately with subsequent dissolution.

The basic idea of this concept of compression is to compress CO<sub>2</sub> in presence of water spray, this will lead to beneficial effects that will reduce the energy demand of the whole compression process:

- Almost isothermal behaviour of compression: the much higher heat capacity of the water respect to CO<sub>2</sub> manage to absorb the heat generated during the gas compression with a neglectable temperature rise of the mixture.

- Reduction of the CO<sub>2</sub> gaseous moles amount during the process: the increase of pressure will enhance also the CO<sub>2</sub> solubility in water that will allow a progressive reduction of the gaseous mole because of dissolution into the liquid, in this way the compression work is strongly reduced.

In Figure 5 is provided a typical cycle evolution of the simultaneous compression/dissolution process.

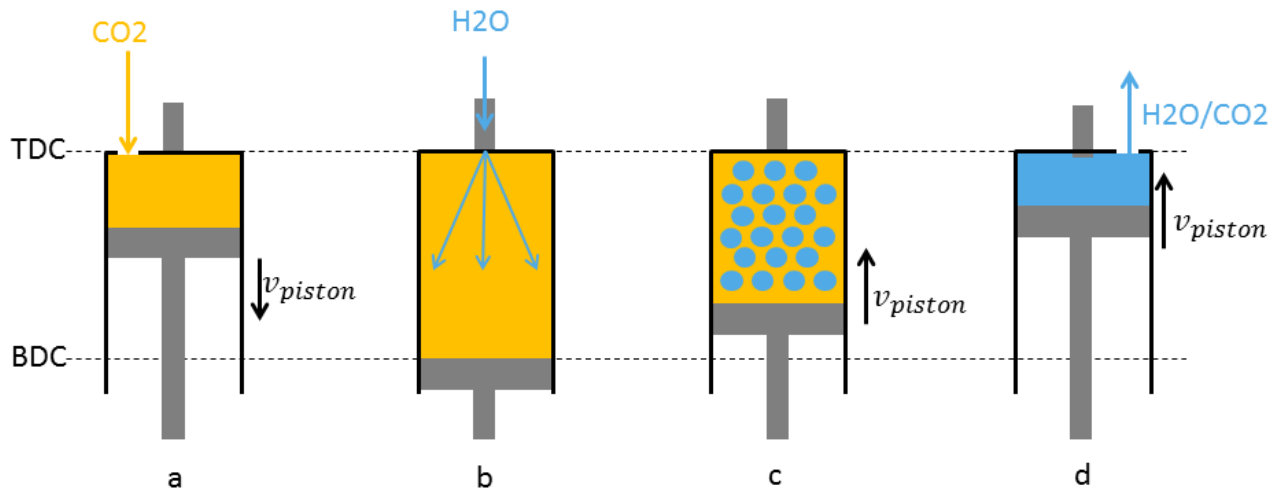


Figure 5 piston compressor with integrated nozzle for simultaneous compression/dissolution process

An exemplary work cycle starts with the piston at the top dead centre, during the first step (a) the piston goes down and CO<sub>2</sub> enters the chamber for difference of pressure, in the second phase (b) water is injected by the nozzle and the mixture starts to be compressed (c) till the point in which ideally saturation is achieved and all the gaseous phase is dissolved inside the liquid (d), taking into account that the amount of injected water has to be calculated in order to allow total dissolution of the gas in water.



## 2 Theory and literary review

### 2.1 Theory

In this chapter is provided a brief introduction for the main physical phenomenon involved into the compression/dissolution process; the aim is to understand which are the key parameters of the process in order to carry out the experimental activity in the best way.

#### 2.1.1 CO<sub>2</sub> Dissolution

Solubility is a chemical property referring to the ability of a solute to dissolve inside a solvent. The solubility of a substance fundamentally depends on the chemical properties of the solute and of the solvent as well as pH, polarity of the molecules and chemical bond, but also on physical properties as well as temperature and pressure. In this case the interest is in the analysis of gas dissolution inside a liquid, in particular of CO<sub>2</sub> inside water; the topic was deeply studied in the early 19<sup>th</sup> century by William Henry. According to the Henry's Law, in equation 2.1 the amount of a given gas dissolved in liquid, at a constant pressure, is directly proportional to the partial pressure of the gas in equilibrium with the liquid [5]:

$$p = k_H(T) \cdot x \quad (2.1)$$

Where:

$p$  is the partial pressure of the solute above the solution,  $x$  is the concentration of the solute inside the solution,  $k_H(T)$  is the Henry's Law constant depending on temperature, usually expressed in atm/mol.

The influence of the temperature is assessed by multiple equations, one is the Van't Hoff equation here showed in equation 2.2:

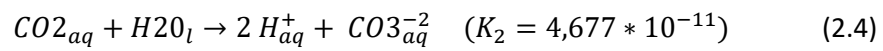
$$k_H(T) = k_H^0 * \exp\left(-C * \left(\frac{1}{T} - \frac{1}{T^0}\right)\right) \quad (2.2)$$

Where:

C is a constant measured in Kelvin,  $T^0$  is the standard temperature

A good collection of values for Henry coefficient in water is provided by Sander [6]. It is important to underline that Henry's law represents only the physical absorption of the gaseous phase, but often also the chemisorption could occur to this process and this can bring to a relevant error to the real case. In the case of water and CO<sub>2</sub> the chemisorption is not so influent but it gives a minimum pH change, by knowing the constant of the reaction involved can be used to understand the concentration of CO<sub>2</sub> in it dissolved.

In equation 2.3 and 2.4 [7] are provided the two more probable chemical reaction that occur between CO<sub>2</sub> and water



Calculations about the Henry's Law are provided in Chapter 3.2 (Water amount calculation).

### 2.1.2 Atomization and Spray

A liquid jet coming out from a nozzle into an ambient gas may breakup into small drops when it is subjected to several external disturbances. These disturbances are generated by different parameters such as surface displacement, pressure or velocity in the supply system, pressure difference with the gas environment and of course by the properties of the specific liquid such as viscosity or surface tension coefficient; this means that the instability and the breakup way of the liquid jets into droplet has a complex behaviour that depends on several parameters. The study of atomization and of the fragmentation technique was developed at the beginning of the nineteenth century in order both to improve the combustion phenomenon and to increase the liquid-gas interface and so the efficiency of the whole process. Nowadays, the use of this technology ranges over this limited application and includes also agriculture, medicine, deposition process, painting,

air-conditioning, etc. Some base law together with the main parameters that rule the process, will be introduced [8].

### Surface tension and surface energy

The splitting process of the droplets, usually starts with the presence of oscillations that can amplify themselves and disintegrate the initial jet. In order to enhance these oscillations, energy is given to the jet in terms of kinetic and mechanical ones through the increase of pressure and also of velocity or by vibrating or in motion device. In this process, the capillary forces originated by two forces including the surface tension and the inertial forces, due to velocity slip between the two phases, together with the viscosity, act in order to reduce the instability of the deformed liquid structure. The main parameters in this process include surface tension ( $\sigma$ ), density of the medium ( $\rho$ ) and its viscosity ( $\mu$ ). The forces of mutual attraction of the molecules could be seen as the reason of the surface tension occurrence. As shown in Figure 6, a molecule far from the free surface is attracted by all the molecule around. The forces are oriented in an isotropic way, so the resultant is null, but a molecule in the surface is attracted just from the molecule inside the liquid, this means that the molecules on the interface seek to sink inside the liquid and the discontinuity surface seek to reduce itself. The surface can be imagined like an elastic membrane in which a surface tension is developed.

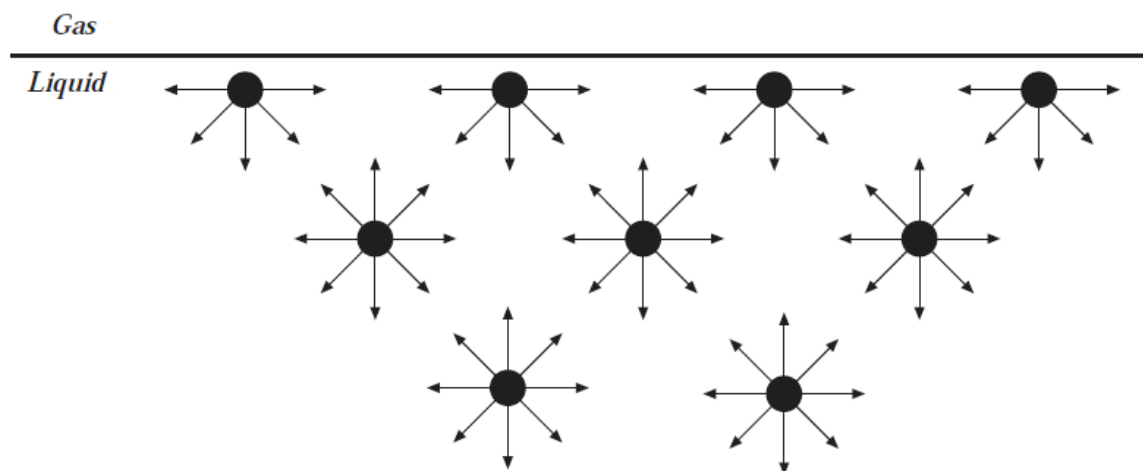


Figure 6 mutual attraction of liquid molecules at interface [8]

The reaction of the surface tension to some perturbation at the interface is the generation of a capillary pressure that fights against this perturbation. The equation that links this pressure to the geometric characteristic of the interface is the Laplace equation. For example, for a sphere with radius  $R$  the surface energy will be  $\sigma 4\pi R^2$  [8].

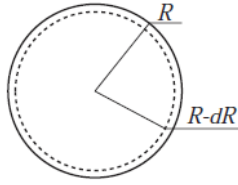


Figure 7 variation of sphere radius [8]

The variation of energy associated to a variation of the sphere radius, showed in Figure 7, will be  $8\pi R\sigma dR$ . At the equilibrium the reduction of surface energy, due to the radius reduction, will be balanced by a pressure variation  $\Delta P$  at interface. The work carried out by the surface tension to balance this pressure will be  $\Delta P 4\pi R^2 dR$  follows:

$$\Delta P 4\pi R^2 dR = 8\pi R\sigma dR \quad (2.5)$$

And so:

$$\Delta P = \frac{2\sigma}{R} \quad (2.6)$$

This relation is the Laplace equation for a spherical interface which represents the capillary pressure that is carried out by the surface tension at the interface for a spherical droplet. In case of infinite cylinder with radius  $R$  the Laplace equation will become:  $\Delta P = \frac{\sigma}{R}$  and more in general the capillary pressure for any surface is given by the ratio between the surface tension and radius of curvature. For this reason, the effect of the surface tension will be bigger for smaller characteristic dimension of the considered liquid. Values of the surface tension for the biggest part of the organic liquid (with reduced Temperature  $Tr = T/T_c$  between 0,4 and 0,6) vary between 2 and  $4 \times 10^{-2} Nm^{-1}$ ; the surface tension of water is:  $7,288 \times 10^{-2} Nm^{-1}$  for a temperature of 20° C [8].

### Atomization efficiency

The process to transfer energy (mechanical or other) in surface energy,  $E_s$  is not a completed process, part of the fed energy,  $E_a$  remains in form of kinetic energy  $E_c$ , and so:

$$E_a = E_s + E_c \quad (2.7)$$

It is also possible to define an efficiency of the atomization process according to equation 2.8:

$$\eta_a = \frac{E_s}{E_a} \quad (2.8)$$

Usually the value of  $\eta_a$  is generally very small and the atomization processes are not so efficient, even if in several combustion phenomena it is good to have high kinetic energy in order to enhance thermal exchange and mixing with air, in our case we just need to have the maximum of surface energy transferred [8].

### Surface waves

As previously mentioned, the mechanism of breakup of a droplet or a jet is linked to the onset of oscillator surface waves at the interface. These oscillator waves have a low wave amplitude and his propagation speed depends on their wavelength; this means that depending on the geometry and on the properties of the liquid, some oscillations could amplify and other could be mitigated by dissipative effects (e.g viscosity). It is possible to obtain information on the characteristics of these oscillations making some dimensional analyses. The forces per unit volume that act in the inner part of the liquid, in absence of external forces are:

- Capillary forces: It is due to the surface tension that, as already seen, leads to a capillary pressure  $\frac{\sigma}{L}$  and a capillary force:

$$F_c = \frac{\sigma}{L^2} \quad (2.9)$$

- Gravitational forces: They generate a force:

$$F_G = \rho g \quad (2.10)$$

- Viscous forces: They act in order to mitigate the oscillations and they generate a force:

$$F_v \propto \frac{\mu V}{L^2} \quad (2.11)$$

- Inertial forces: They are due to the relative speed between gas-liquid and generate a force:

$$F_I \propto \frac{\rho_l V^2}{L} \quad (2.12)$$

In these expression L represents a characteristic dimension of the considered liquid structure and V the velocity of the oscillator wave. If we consider to apply a wave impulse at the interface, the capillary forces  $F_C$  and the gravitational ones  $F_G$  will fight against the wave propagation and that seek to establish again the initial condition. When these two forces are similar is possible to write:

$$F_G \cong F_c \rightarrow \rho g \cong \frac{\sigma}{L^2} \quad (2.13)$$

This allows to define a characteristic length of the oscillations in this condition, called capillary length:

$$L_c = \sqrt{\frac{\sigma}{\rho g}} \quad (2.14)$$

Oscillations with wavelength ( $\lambda = 2\pi L$ ). bigger than  $L_c$  will be governed by gravitational forces, while if wavelength are smaller than  $L_c$  will prevail capillary forces. Roughly it is possible to say that “long” waves are more gravitational while “short” waves are more capillary. If we consider that there are gravitational waves in steady condition it will be

$$F_G \cong F_I \rightarrow \rho g \cong \frac{\rho V^2}{L} \rightarrow V \cong \sqrt{Lg} \quad (2.15)$$

The viscous forces will be negligible if

$$L \gg L_{DC} = \frac{\mu^2}{\rho\sigma} \quad (2.16)$$

Where  $L_{DC}$  is the dissipation length of capillary waves. Ultimately the capillary waves will exist under the condition [8]:

$$L_{DC} \ll L \ll L_C \quad (2.17)$$

### External forces influence and dimensionless number

Until now, only the inner force in the liquid were be considered. These allows to study breakup mechanism if they are dominant, so for small relative speed between gas and liquid ( $\approx 1\text{m/s}$ ). When the speed become bigger, the aerodynamic forces at the interface are the mainly relevant in the atomization process. These forces are usually indicated as  $p_g$  and  $\tau_g$ , as showed in Figure 8

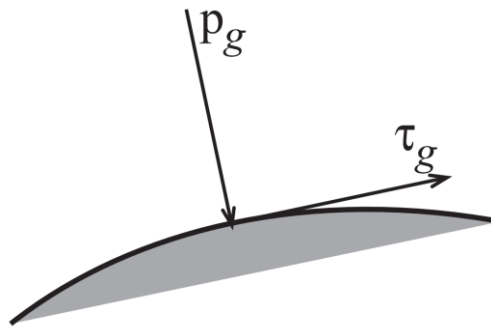


Figure 8 aerodynamic forces at the interface liquid/gas

$P_g$  acts perpendicularly at the interface and fights against the capillary pressure, generated from the forces due to the surface tension, it sustains and amplifies the oscillations;  $\tau_g$  instead acts tangentially to the surface and acts in order to remove liquid droplets from the jet. Both these forces are proportional to the dynamic pressure of gas, calculated as  $\frac{1}{2}\rho v^2$  in which  $v$  is the relative velocity between gas and liquid. Now that the main forces that characterize the atomization process are defined, is possible to define some dimensionless group that are really helpful in order to understand which are the dominant forces and when the various correlation has sense to be used.

An important measure of the relative dynamic pressure respects to the capillary pressure is given by the Weber dimensionless group described as:

$$We_g = \frac{\rho_g v^2}{\frac{\sigma}{D}} = \frac{\rho_g v^2 D}{\sigma} \quad (2.18)$$

It can be considered as an index of the possibility to atomize a liquid. Sometimes, most in the rupture process of a liquid jet, the Weber number can be referred to the liquid and not to the gas phase:

$$We_l = \frac{\rho_l v^2 D}{\sigma} \quad (2.19)$$

In this case it represents a measure of the ratio between the inertial forces and the capillary forces. In addition, the viscous forces in the liquid fight against the breakup; in this case the dimensionless number that give a measure of the atomization possibility is:

$$Oh = Z = \frac{\mu_l}{\sqrt{\rho_l \sigma D}} \quad (2.20)$$

This represents the Ohnesorge number that can be considered (under the dimensional point of view) like the ratio:  $\sqrt{We}/Re$ . All the quantity in the Ohnesorge number are generally referred to the liquid, so it depends just on the thermodynamic condition of the fluid to be atomized [8].

### **Conclusive considerations and application**

From the analysis of the forces that rule this process, it is clear that the characteristics of the medium that influence the breakup process are according importance:

Surface tension, Viscosity, Density and Environmental pressure.

This kind of measurement is performed in order to understand the droplet size distribution of the spray obtained by the real atomizer. A common measure of drop size distribution is the Sauter Mean Diameter which gives the diameter of a drop with the same surface/volume ratio as the whole spray:

$$D_s = \frac{1}{\sum \frac{f_i}{d_i}} \quad (2.21)$$

Where:

$f_i$  is the scalar variable for the dispersed phase and  $d_i$  is the value of the droplet diameter.

To better understand how the spray will be formed, in literature is provided an empirical correlation [9] provided in equation 2.22 that gives an estimation of SMD

$$SMD = 2.25\sigma^{0.25}\mu_L^{0.25}\rho_A^{-0.25}\dot{m}^{0.25}\Delta P_L^{-0.5}\rho_A^{-0.25} \quad (2.22)$$

Where:

$\sigma$  is the surface tension,  $\mu_L$  the liquid viscosity,  $\dot{m}$  the liquid flowrate,  $\Delta P_L$  the pressure difference between gas and liquid and  $\rho_A$  the gas density.

### 2.1.3 Water gas Interface

In order to understand how the dissolution process evolves it is important to make some considerations about the diffusion phenomenon that occurs on the interface between gaseous phase and liquid droplets. The simplest description of the diffusion phenomenon is provided by the Fick's law developed by Adolf Fick in the 19<sup>th</sup> century. The first Fick's law relates the diffusive flux with the concentration under the assumption of steady state process. It is expressed by equation 2.23:

$$J = -D \frac{\partial \varphi}{\partial x} \quad (2.23)$$

Where:

$J$  is the diffusion flux that measures the amount of substance that flow through a unit area during a time interval,  $D$  is the diffusion coefficient or diffusivity,  $\varphi$  is the concentration and  $x$  represents the length in which the transport of mass occurs (unidirectional in this case) [10].

In the compression/dissolution application we know from the Henry law the concentration that will be reached at the equilibrium for a certain pressure and we want to investigate the dynamic of the phenomenon in order to understand the droplet diameter required to have the best dissolution performance according to the speed of the piston.

This means that we are interested in how the diffusion occurs during time. This is described by the second Fick's law in equation 2.24 [10]

$$\frac{\partial \varphi}{\partial t} = D \cdot \nabla^2 \varphi \quad (2.24)$$

Where:

$\frac{\partial \varphi}{\partial t}$  represents the variation of concentration during time and  $\nabla^2 \varphi$  represent the Laplacian operator of concentration over the considered dimensions.

In the compression/dissolution case the water droplets shape can be assumed to be spherical which means that  $\nabla^2 \varphi$  can be expressed in spherical coordinate according to equation 2.25 [11]

$$\nabla^2 \varphi = \frac{1}{r^2} \frac{\partial \varphi}{\partial t} \left( r^2 \frac{\partial \varphi}{\partial r} \right) \quad (2.25)$$

Where  $r$  is the ray of the sphere.

A solution of the differential equation is provided in equation 2.26 [12]. The solution is valid under the condition that the droplet has always the saturation (Henry) concentration constant over all the surface

$$\frac{\theta(r, t) - \theta_{inf}}{\theta_0 - \theta_{inf}} = 2 \cdot e^{-3.1516^2 Fo} \frac{\sin\left(3.1516 \frac{r}{R}\right)}{3.1516 \frac{r}{R}} \quad (2.26)$$

Where:

$\theta(r, t)$  is the concentration of CO<sub>2</sub> in water in function of the radius of the droplet and in function of time,  $\theta_{inf}$  is the concentration that is achieved for a given pressure in steady conditions (known from Henry's law),  $\theta_0$  is the concentration at the beginning of the diffusion process,  $Fo$  is the

Fourier number defined as  $FO = \frac{Dt}{L^2}$  where  $L$  is the characteristic length that in this case is the sphere radius, the Fourier number gives us information on the ability of the gas to diffuse into the droplet body. Applying this correlation to the compression/dissolution unit is possible to establish the dimension of the droplets needed in order to reach a desired percentage of the Henry's concentration (reached for steady conditions) in a limited amount of time.

The available time for the compression has to be calculated according to the speed range of the piston (0.016-0.12 m/s from experimental measurement). Considering the stroke of 571.5 follows that the available time is in the range  $\approx 4.7-36.2$ , is also possible to define the mean time required to increase the pressure of 1 bar. The pressure range is 9 bar so is possible to calculate  $\Delta t_{step}$  that is in the range 0.53-4.02 s/bar respectively for low and high piston speed.

At this point is possible to decide a percentage of dissolution to achieve in a step of compression (respect to the steady condition and calculate the Fourier number according to Equation 2.8, knowing the time required for the pressure increase of 1 bar from the Fourier number is easily possible to calculate the radius of the spherical droplet. The results of this procedure are provided in Table 1

*Table 1 Droplet diameter for a given percentage of dissolution during the transitory of 1bar pressure increase*

$\frac{\theta(r, t)_{r=0} - \theta_{inf}}{\theta_0 - \theta_{inf}}$	$FO = \frac{Dt}{R^2}$	Droplet radius [ $\mu m$ ] Max speed	Droplet radius [ $\mu m$ ] Min speed
<b>0.0001</b>	1	31.9	87.8
<b>0.001</b>	0.76	36.6	100.8
<b>0.01</b>	0.54	43.4	119.5
<b>0.1</b>	0.3	58.2	160.4
<b>0.45</b>	0.15	82.3	226.8

This is a rough estimation that doesn't take into account turbulence phenomenon or water layer formation but gives an idea on how the droplet diameter affects the dissolution phenomenon in terms of percentage with the ideal case, this analysis is helpful in order to select the nozzle taking into account the available dissolution time depending on the piston speed.

In order to enhance this process apart the droplet size is also important to guarantee a low enough volume ratio that can be defined according to equation 2.27

$$v(T, p) = V_{H_2O}^0 / V_{CO_2}^0 \quad (2.27)$$

Where:

$V_{CO_2}^0$  is the CO<sub>2</sub> volume that correspond with the chamber volume,  $V_{H_2O}^0$  the volume of the injected water.

This ratio has to be kept as low as possible in order to obtain a disperse enough mixture, if not a dense spray will occur characterized by coalescence that will lead to much larger water drops; this observation influence the choice of the chamber geometry and of the nozzle characteristic. The selection of the injector determines the spray pattern and consequently the quality of the dissolution process.

#### 2.1.4 Thermodynamics of compression

As previously introduced, the common method for the dissolution of CO<sub>2</sub> is the compression of the gaseous phase with subsequent dissolution. This means that the comparison term is the isentropic compression of the gas with the addition of the work to compress the liquid [13]:

$$W_{isentrop} = \frac{\kappa p_0 V_0}{\kappa - 1} \left( \left( \frac{p}{p_0} \right)^{\frac{\kappa-1}{\kappa}} - 1 \right) \quad (2.28)$$

Where:

$W_{isentrop}$  is the work to compress the gas in an isentropic transformation

$\kappa$  is the ratio of the specific heat at constant pressure over the specific heat at constant volume  $\frac{c_p}{c_v}$

$p_0 V_0$  are the initial pressure and volume

From the enthalpic form of the first principle of thermodynamics for an adiabatic system is possible to evaluate the ideal work to increase the pressure of the water as [14] :

$$W_{liquid} = \Delta H = V_{H_2O} \Delta p \quad (2.29)$$

Where  $\Delta H$  is the difference of enthalpy,  $V_{H_2O}$  the volume of the water with the hypothesis of constant density during the process and  $\Delta p$  the increase of pressure needed.

The work calculations for the compression/dissolution unit are developed in Chapter 4.3.

## 2.2 Literature review

In this chapter a small overview over the state of the art on the CO<sub>2</sub> dissolution is provided, from there the need to perform further investigation about the dynamic process of dissolution; follow some example found in literature about compression/dissolution of gases in liquid.

The CO<sub>2</sub> dissolution in water is a process involved in various scientific and technological fields. It is a topic of great interest and in particular in the field of natural geologic process like CO<sub>2</sub> disposal in the sea or in sedimentary formation, beverage industries and carbon capture and sequestration. For most of these application, it is so needed to have data about the Henry's constant for temperatures up to 100 °C and pressures up to 100 MPa. Because of this, a big number of experimental studies were performed in order to create a database that could allow to have information for different temperatures and pressures. In 1981 D. Mackay et al. assembled and reviewed the previous available data on solubility in a whole work [15]. In 1992 Carroll et al. [16] compiled the results for investigations based on the Henry's law temperature lower than 100°C and pressure lower than 1 MPa.

These were just the most relevant works but numerous experimental studies about this topic can be found in the literature. What is pointed out most from the analysis of all these works is that there is a consistent difference in the provided data by different authors. Although the results are provided with uncertainties, generally of the order of a few percent, comparison of different studies reveals differences sometimes bigger than 10 % for the same pressure and temperature conditions. This means that there are present evidently unrecognised systematic errors in at least some of the studies and there is the need to understand what causes this deviation in the dissolubility evaluation. It is also important to mention that while the definitions of dissolution coefficient needs to be improved, as far as the dynamic process of compression/dissolution it is not easy to find relevant and exhaustive works in the existing literature.

The increasing investment on the power to gas technology will determine a bigger interest in the use of simultaneous compression/dissolution processes to produce CO<sub>2</sub> enriched flows to feed for example electrolysers as in the CELBICON case. At the moment in literature it is possible to find fixed values of dissolution coefficients for different pressure and temperature values at equilibrium, once the steady process is achieved. Then the need to investigate how the dissolution evolves during the dynamic compression process for different range of pressures has to be investigated.

Compressors that use liquid injection for cooling to absorb the temperature increase, have already been investigated in the last century. A large amount of inventions and patents are registered about this technology, the most significant will be briefly described.

Zahm et al (USA 1938) was one of the first to build and register the patent [17] of a device able to compress gas in which liquid was injected in order to absorb the heat generated during the compression Wilfred J Rouleau (USA 1947) [18] invented another device to compress air or other gases with liquid injection to control the temperature, in this case some of the compressed gas is used to force a cooling spray into the chamber, in this way part of the useful effect is wasted but anyway the thermodynamic benefit is preserved, a section of the invention is provided in Figure 9.

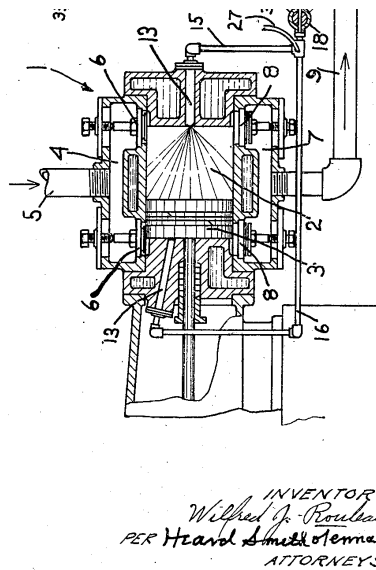


Figure 9 Liquid injection compressor Inventor Wilfred J Rouleau US patent [18]

Winandy and Lebrun (2002) [19] had also positive results in the energy saving of compression comparing normal injection with vapour and liquid injection for a scroll compressor. What is possible to understand from these experience is that in the most cases high energy efficiency is achieved. The need of the lubricants is eliminated and also the contamination of the gas is avoided. The problem that could have avoid the spread of this technology at a commercial scale is probably the increased number of component and higher investment costs respect to the normal compression.

The common element in most of these investigated case is that the liquid was something used just for its cooling and/or lubricant effect, it is not easy to find in literature a case of compression with liquid which goal is to create a flux with gas dissolved in the liquid. The growing interest at the power to gas technologies allows to address always more importance at the preparation of this kind of flows CO<sub>2</sub> enriched, for this reason the Karlsruhe Institute of Technology in collaboration with M.T.M (company in Turin, Italy) developed a patent and built a first prototype showed in

Chapter 393.1 (Experimental setup). The use of this technology addressed to the production of CO<sub>2</sub> enriched flows, could determine a faster marked penetration of this kind of compressors.



### 3 Experimental setup and procedure

#### 3.1 Experimental Setup

In this paragraph, the main components of the experimental setup are presented, giving attention to the used sensors to get the data and their measurement error. Figure 10 and Picture 1, show respectively a scheme and a picture of the setup. It is possible to see that the whole experimental setup is subdivided in three different areas: Hydraulic unit (A), Compression/dissolution unit (B) and the Injection system (C). In Figure 10 it is provided a scheme of the experimental setup where it is possible to recognize the three different areas. The Hydraulic unit through a pump increases the pressure of the oil which, by using an actuated three way valve allows the movement of the piston. The Injection system increases the pressure of water until the required value required at the nozzle and inside the piston. CO<sub>2</sub> from the bottles and atomized water enter the compression/ dissolution unit so the CO<sub>2</sub> can be dissolved. In Picture 1 is also provided a photo of the experimental setup as it stands in the lab.

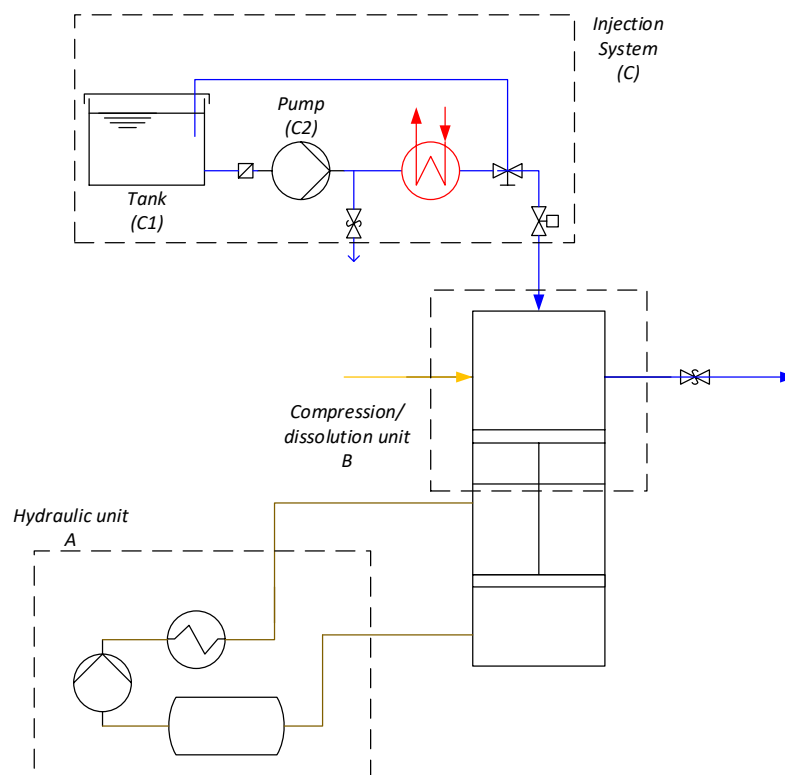
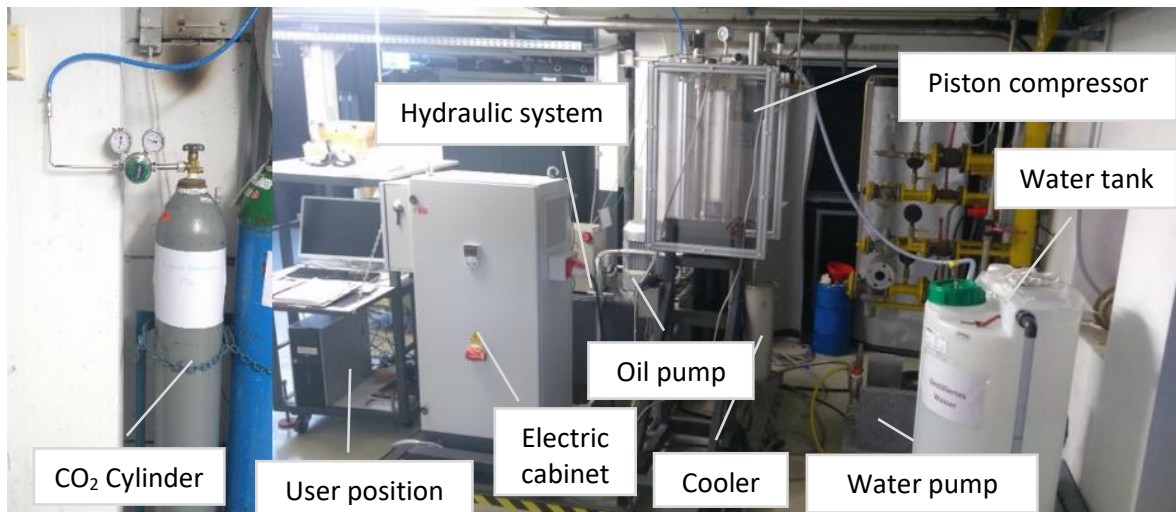


Figure 10 Components diagram of the experimental setup



Picture 1 CO2 cylinder at the left, hydraulic system(A) and compression/dissolution unit (B in the center), and injection system (C) at the right

It is possible to describe the experimental setup according to the following subdivision:

**1. Hydraulic unit (A)**

The hydraulic unit works to change the oil pressure that allows to control the piston movement. It is shown in Picture 2, while in Table 2 the main specifications of the unit are provided.



Picture 2 Hydraulic unit: oil pump at the right and oil fan cooler at the left

Table 2 Hydraulic unit, main specifications

<b>Oil Pump</b>	
<b>Power [kW]</b>	18
<b>Maximum pressure [bar]</b>	135
<b>Max Flowrate [l/min]</b>	73
<b>Oil Cooler</b>	
<b>Power [W]</b>	115-150
<b>Valves</b>	
<b>typology</b>	Electro-valves 3/2 ball valves with pneumatic actuator

The pump has an inverter allowing the variation of the piston speed also during the compression.

## 2. Compression/dissolution unit (B)

The compression/dissolution unit is the main component of the setup. An image of the piston is provided in Picture 3. The cylinder is optically accessible in order to allow the investigation of the spray pattern and the dynamics of the injection/compression through optical measurement techniques like phase Doppler anemometer, Back-illuminated optical imaging or Planar Laser-induced Fluorescence. Its main specifications are provided in Table 3.

Table 3 Piston compressor specifications

<b>diameter</b>	<b>125 mm</b>
<b>stroke</b>	600 mm
<b>volume</b>	7.3631 l
<b>electric engine</b>	7.5 kW
<b>Compression cycle per minute</b>	3 – 7
<b>piston speed</b>	16 – 140 mm/s



*Picture 3 Piston compressor*

The pressure inside the cylinder is measured with a pressure gauge sensor working in the range of 0-25 bar, with an accuracy of  $\pm 0.1\%$  in the range of the required operational parameters. Also, the temperature is measured with a type K thermocouple welded inside the chamber. The position is measured with an embedded sensor, which by exploiting the principle of magnetostriction [20] gives results with an error of 0.002% of the full scale of 2500 mm.

### **3. Injection system (C)**

The injection system (C), provide pressurized water at the nozzle in order to atomize the water inside the piston chamber. In Picture 4 is possible to see the water storage tank at the right. It has a volume of 200 L and it is filled with water that is purified through a carbon filter. The temperature of the water is measured with a type-K thermocouple in order to control its temperature. After the tank, a bag filter is placed to clean the water (also visible in Picture 4). Then, the water is sucked in the pump that is equipped with a pressure regulator needed to dump the pressure peaks. The specifications of the pump are provided in Table 4.



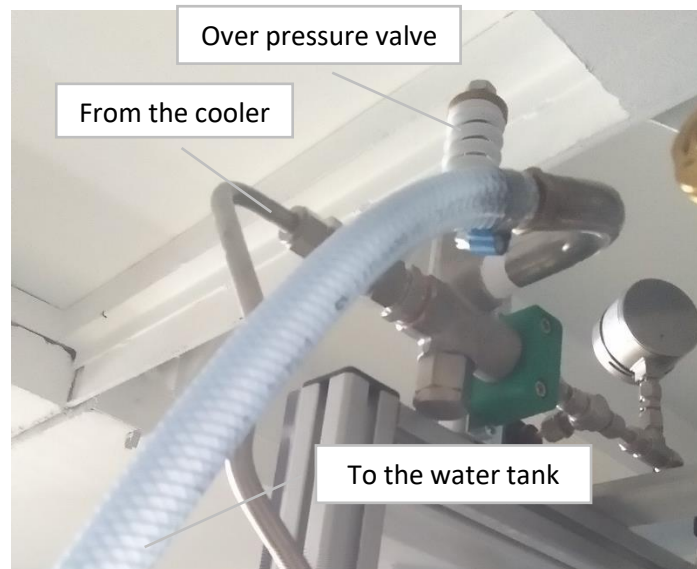
Picture 4 Injection system, water pump filter and water tank

Table 4 Pump and pressure regulator specifications

<b>Electric pump</b>	
<b>Maximum pressure</b>	100 bar
<b>Power electric engine</b>	7.5 kW
<b>Maximum flowrate</b>	1457 lh <sup>-1</sup>

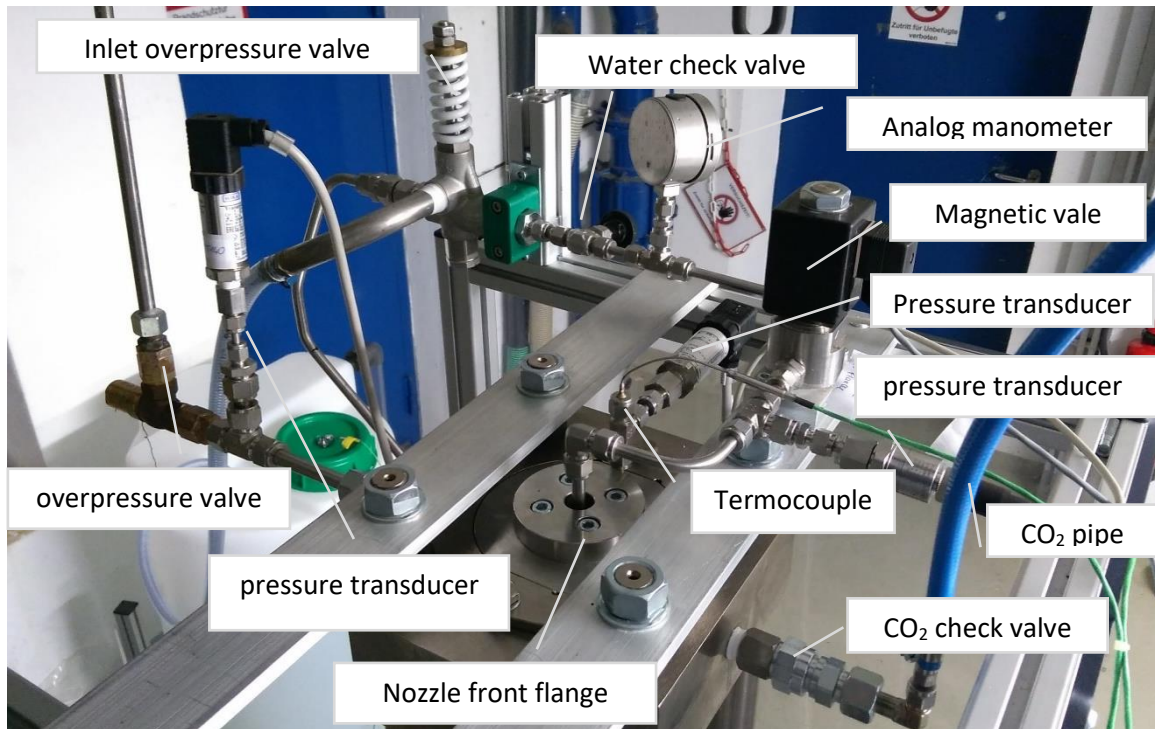
From Picture 1 (overall setup) is possible to see cooler, it is located just after the pump in order to mitigate the overheating effect from the pump. Cold water from the central network (variable temperature) is used as the cooling medium.

Looking at Picture 5, it is possible to see the pump recirculation branch and the overpressure valve. This valve allows water flow just when the water pressure reaches the pressure value set in the valve, this value can be manually adjusted. It can be varied between 30 and 100 bar which corresponds to a flowrate from 5 to 30 l/min.



*Picture 5 injection system, recirculation branch and overpressure valve*

After the overpressure valve, as visible in Picture 6 the pressure of the water is measured first by an analogic manometer and after by a gauge pressure sensor working in the range of 1-100 barg with a measurement error of 0.5% of the range. The injection is regulated by a magnetic valve working until 250 bar, it is powered by the electric cabinet. The valve position (open or close) is regulated by an internal electrically actuated piston, the delay time from the electrical signal to the actuation is 0.2 s for opening and 0.5 s for closing [21].



Picture 6 injection, CO<sub>2</sub> and exiting line located on the top of the piston

The last component of the Injection line is the nozzle. After a careful evaluation of all the nozzle typologies available in the market was decided to use the full-cone spray, a concept of this nozzle typology is showed in Figure 11.

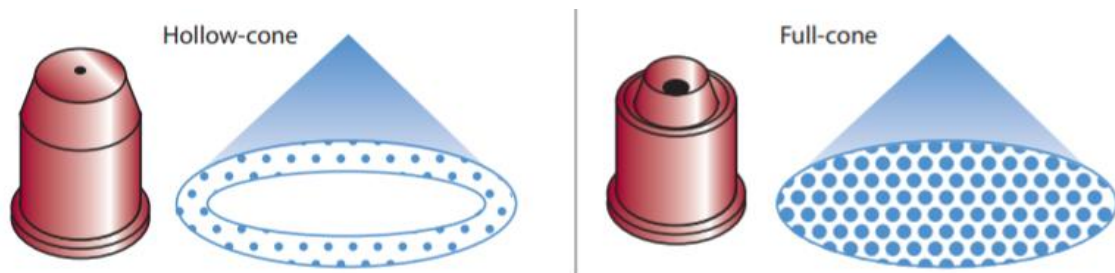


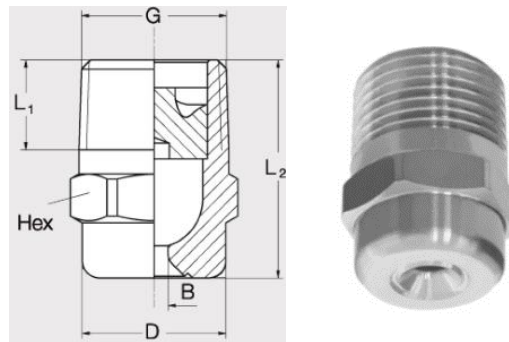
Figure 11 spray pattern for hollow-cone at the left and Full-cone at the right [22]

Even if other nozzles like the hollow cone ones show a smaller droplets diameter, the full cone nozzle was chosen because of more uniform distribution in the chamber [22].

Two different models were examined in this study. They are provided by Lechler [23]. In Table 5 the main nozzles specifications are presented and in Picture 7 is possible to see an image of the nozzle with its technical drawing. For the two models, just the technical dimensions are different.

Table 5 Nozzles technical specifications

	Nozzle 1	Nozzle 2
<b>Model</b>	<b>490.403 1Y</b>	<b>490 444 1Y CA</b>
<b>Nozzle typology</b>	<b>Axial full cone</b>	<b>Axial full cone</b>
<b>Orifice diameter (B) [mm]</b>	1.244	1.244
<b>Angle [°]</b>	45	60



Picture 7 nozzle image and technical drawing

The CO<sub>2</sub>, stored in cylinder at 49.5 bar, enters the chamber (blue pipeline in Picture 6) through a check valve (0.3 bar pressure difference) when the piston goes down and creates vacuum inside the chamber. During the compression process, the solution of CO<sub>2</sub> and water is expelled towards a tank located outside of the lab. In a new configuration of the experimental setup it will be stored in a buffer tank at 10 bar. The pressure value of the exiting flux is given by an overpressure valve set at 10 bar according to the CELBICON requirement. It can be manually adjusted in the range of 10 to 40 bar. This flow represents the product of the process that will be stored in a pressurized vessel in order to feed the electrolyser.

Concerning the atomization of the procedure, sensors are connected with the electric cabinet for power supply and with NI-DAQ platform that allows to read the current values from the computer. Every sensor gives a current output in the range 4-20 mA that is converted from current signal to digital from the NI-DAQ platform. Then, the digital signal has a linear dependence with the current value converted in LABVIEW. In order to investigate the dissolution process and the dynamic response of the system, the following values are saved: Time, encoder position, injection pressure, chamber pressure, injection magnetic valve (binary), chamber temperature, water tank temperature, inverter pump (hydraulic unit), valves position (binary) and pressure sensors of the hydraulic unit.

An example of text file in which the experimental data are saved is provided in appendix.

## 3.2 Experimental procedure

As already introduced the aim of this study is to choose the correct parameters in order to achieve the maximum energy saving for the compression/dissolution process. For this reason, two different nozzles and two different velocity profiles of the piston are analysed. The Experimental procedure can be subdivided in the following steps:

### 3.2.1 Water amount calculation

The first parameter to be determined is the amount of injected water. It has to guarantee that all the gas can dissolve until the end of compression (10 absolute bar). This value is evaluated thanks to the following equations (3.1-3.4).

$$k_H = k^\circ \exp\left(\frac{1}{T_{water}} - \frac{1}{T_0}\right) \quad (3.1)$$

$$x = k_H P_{final} \quad (3.2)$$

$$\rho_{CO_2} = \frac{P_{initial}}{RT} \quad (3.3)$$

$$V_{water} = \frac{m_{CO_2}}{x} - m_{CO_2} \quad (3.4)$$

Where  $k_H$  is the Henry constant at  $T_{water}$  25°C,  $k^\circ$  corresponds to the reference Henry constant for  $T_0 = 25^\circ\text{C}$ ,  $P_{final}$  is the pressure of 10 bar,  $x$  represents the number of  $\text{CO}_2$  moles over the mass of the solution,  $V_{water}$  is the amount of water that has to be injected,  $\rho_{CO_2}$  is the  $\text{CO}_2$  density calculated for an initial  $\text{CO}_2$   $P = 1.02$  bar and a  $T = 21^\circ\text{C}$ , (2 °C higher than the measured one in order to take into account warming effects of the chamber),  $R$  is the universal gas constant,  $m_{CO_2}$  represents the mass of  $\text{CO}_2$  inside the chamber.

Table 6 resumes all the values used to evaluate the amount of water.

Table 6 Parameters involved in the water amount calculation

$V_{water}$ [l]	0.8603	$\rho_{CO_2}$ [ $kg_{CO_2} \cdot m^{-3}$ ]	1.8352
$k_H$ [ $mol \cdot kg^{-1} \cdot bar^{-1}$ ]	0.034	$R$ [ $kJ \cdot kg^{-1} \cdot K^{-1}$ ]	0.1889
$T_{water}$ [ $^{\circ} C$ ]	25	$d$ [mm]	125
$x$ [ $mol_{CO_2} \cdot kg_{solution}^{-1}$ ]	0.3399	$stroke$ [mm]	571.5
$T_{CO_2}$ [ $^{\circ} C$ ]	21	$V_{chamber}$ [l]	7.0133
$P_{final}$ [bar]	10	$m_{CO_2}$ [g]	12.8706
$P_{initial}$ [bar]	1.02	$M_{CO_2}$ [ $g \cdot mol^{-1}$ ]	44.095

### 3.2.2 Piston speed evaluation

In order to achieve an improvement of the dissolution process and so of the energy saving, it was decided to perform the experiments according to two different speed configurations. Figure 12 the piston position in function of time for two-speed configuration is showed, it is also possible to see the used inverter value of the hydraulic pump.

First case A was performed, with a piston speed of 67.5 mm/s. This speed value was chosen because it is the one that allows continuous operation of the electric engine of the pump without overheating problems. This speed also fulfils the CO<sub>2</sub> amount required by the CELBICON operation conditions (4-8 kg per day [4]). Case B was built with two different linear slopes. The first piston speed was 111.2 mm/s and after 2/3 of the stroke it was changed to the lowest affordable speed for the inverter that is 15.8 mm/s.

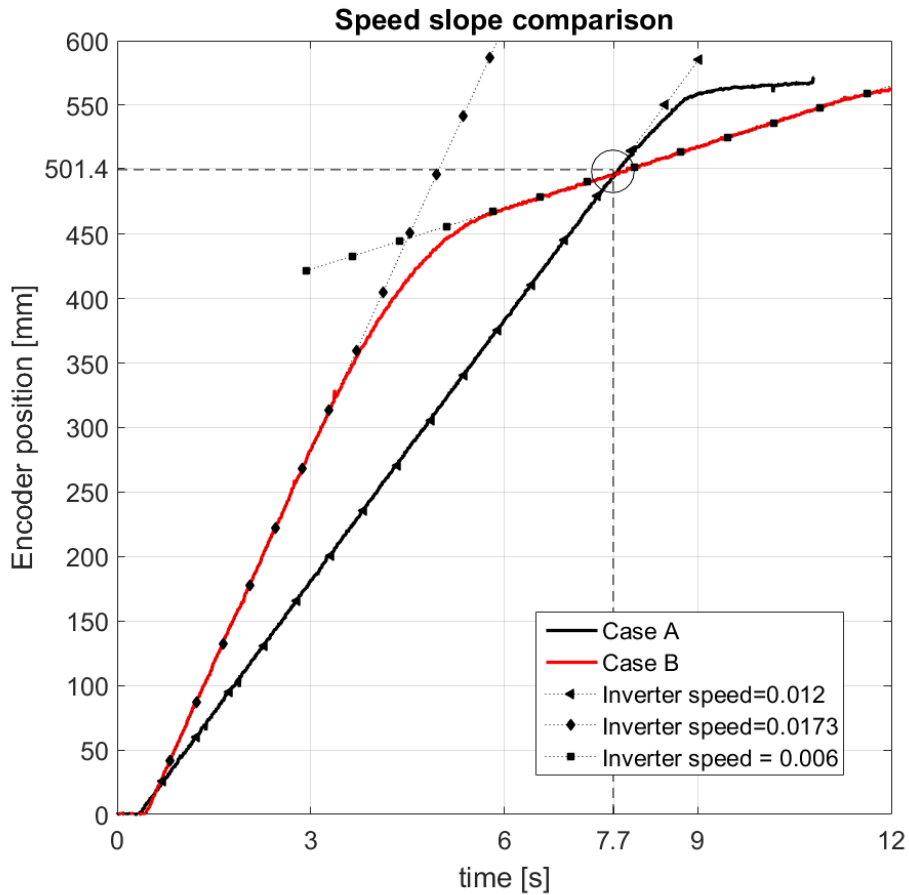
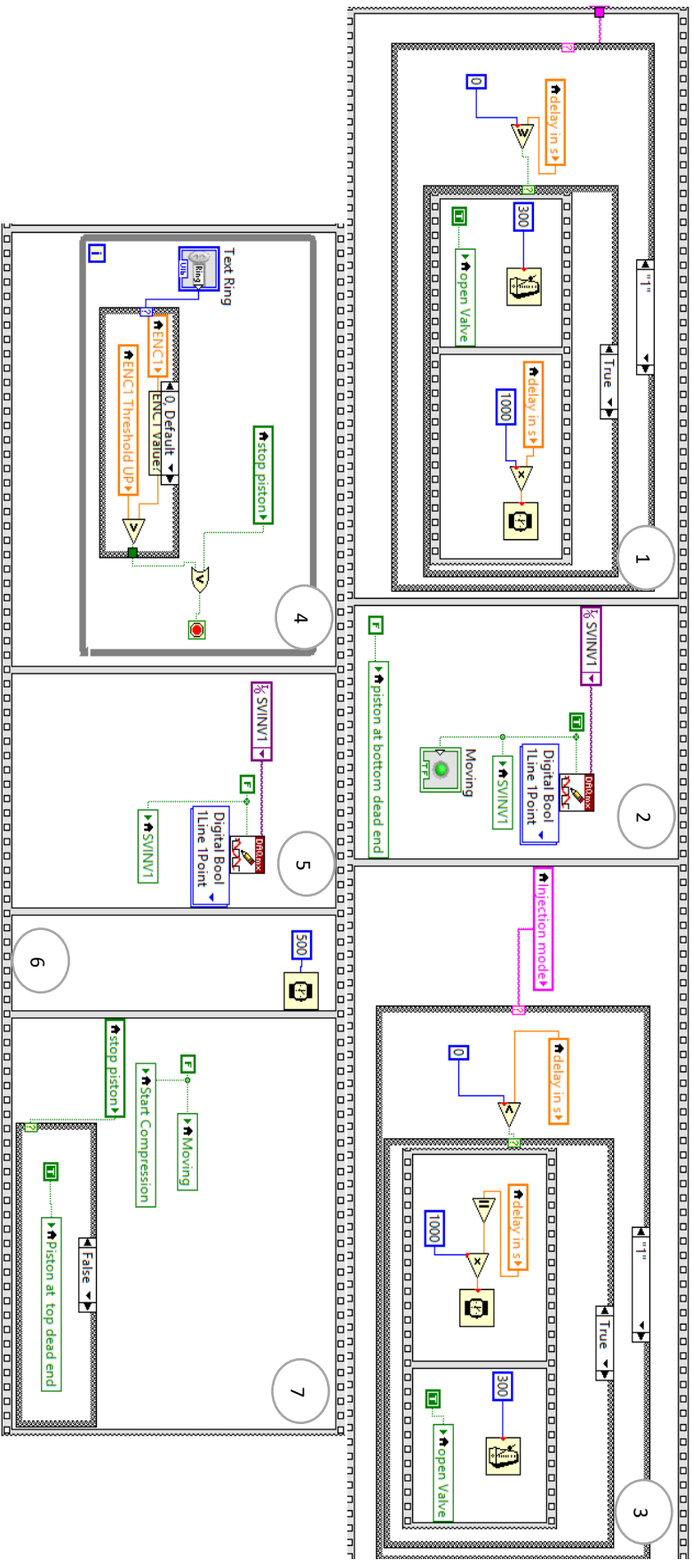


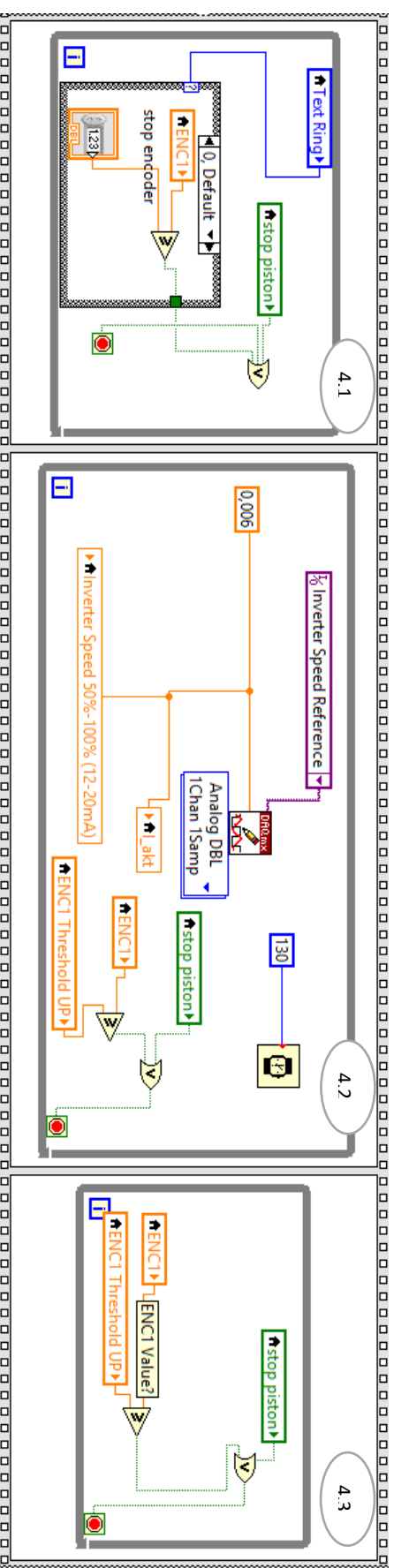
Figure 12 Case A and Case B, speed slope comparison

It is already well known that the longest the dissolutions process lasts, the better results will be achieved, in terms of diffusion phenomenon. For this reason, the injection time became a crucial parameter that needs to be kept fixed in order to compare properly these two cases. For this reason it was decided to inject water until the point where just water is present inside the cylinder. After that point, there is no gaseous phase that can dissolve anymore. This point corresponds to an encoder position of 501.4 mm, it comes out from stroke position minus the height of the injected water. It corresponds to the value in which the two speed configurations meet as is visible in Figure 12. It was obtained from case A, that the injection time was calculated in order to finish the injection when the piston reaches the position just mentioned. The result was an injection time  $t_{inj}$  equal to 7.43 s, but just the total time 7.7 s that takes into account also the initial delay of the control system is visible in Figure 12. In these two cases, the dissolution will be investigated until this injection time (same for the two cases) and this encoder position; for now there is no interest in what happens subsequently. It is important to build the two slopes in order to notice a difference in the dissolution process. In order to do that, it was decided to use a constant speed for case A and a double linear

speed for the case B. In the B configuration the speed is changed after 2/3 of the stroke, this position is chosen in order to have a higher speed when the increase of pressure with increase of encoder position is low and a lower speed in the last compression phase when the pressure increase rapidly for the increase of the encoder position. In order to evaluate the right slope, a first analytical model was built, but several problems occurred: different dynamic response of the system, different initial delay time and different time required to change the speed and different position in which the system receives the signal in order to change the speed. All these problems required to apply an iteratively approach where just the first speed of the B slope was varied until the point in which the two speed profiles meet (7.7 seconds). The chosen value of inverter speed in case A is 0.012 A. Initially, the LabVIEW code that controls the compressor process was created just to have a constant inverter speed during the piston movement. In order to allow a different speed profile a modification in the code was done. In Picture 8 and Picture 9 the initial code to obtain constant piston speed and the required change to obtain the B speed configuration are provided.



Picture 8 LABVIEW code for compression phase with constant speed



Picture 9 LABVIEW code change for variable speed

The main part of the compression phase procedure is shown above. For better comprehension the code is subdivided in 7 windows. The first and the third windows are needed just in case of need to set an injection time shift in respect to the piston movement and can be positive or negative. In the second window the piston starts to move, in window 4 the piston continues moving until the upper threshold of the encoder position is reached, after this it stops in window 5. After this in window 6 a time of 0.5 s is given to take into account the dynamic response of the system and in the last window the upper position of the piston is communicated to the user.

The three windows showed in Picture 9 substitute the fourth window of the code showed in Picture 8, the rest of the code remains the same. Like in case A, the initial inverter speed is already selected before the compression. In window 4.1 the piston continues to go up with the inverter speed previously selected, until the encoder reaches the desired position (for case B 2/3 of the stroke). In window 4.2 once the decided encoder position is reached the inverter receives a signal to change value and becomes 0.006 A (lowest value). After this, from window 4.3 the compression continues with the lowest speed until the upper threshold is reached.

### 3.2.3 Nozzle selection and flowrate evaluation

Another variable of the process, is the nozzle. It is chosen in order to provide the suitable volume flowrate within the limitation of the experimental setup (maximum inlet pressure of 100 bar, minimum overpressure valve value of 10 bar). For each nozzle that will be used, a different inlet pressure will be set in order to reach the same flowrate. The flowrate  $\dot{q}$  is easily determined according to equation 3.5

$$\dot{q} = V_{water}/t_{inj} \quad (3.5)$$

Where:

$V_{water}$  is the water amount and  $t_{inj}$  the injection time previously introduced. Because of different geometrical specifications, each nozzle needs a different value of water pressure in order to reach the same flowrate of 6.94 [l/min]. This value of pressure was calculate according to the producer data [23] and through equation 3.6

$$P_{\dot{q}} = P_1 \cdot \left(\frac{\dot{q}}{Q_1}\right)^{\frac{1}{n}} \quad (3.6)$$

where  $P_{\dot{q}}$  is the pressure to be obtained for the known flowrate ( $\dot{q}$ ),  $P_1$  and  $Q_1$  are the values of the pressure and the flowrate taken from datasheet.

The value of the flowrate was achieved varying the overpressure valve that regulates the inlet flow. For this reason also in this case, in order to achieve the right pressure, a high number of iterations was needed. The flowrate was determined making injection of 7.43 s and reading the height of the water column after each injection ( $\pm 1$ mm measurement error). The final pressure is provided in Table 7 while in Figure 13 the value of water amount obtained from the reading of the water column height just mentioned is provided.

Table 7 Nozzles operational parameters

Nozzle	1	2
pressure [bar]	91	27
$q$ [l/min]	6,94	

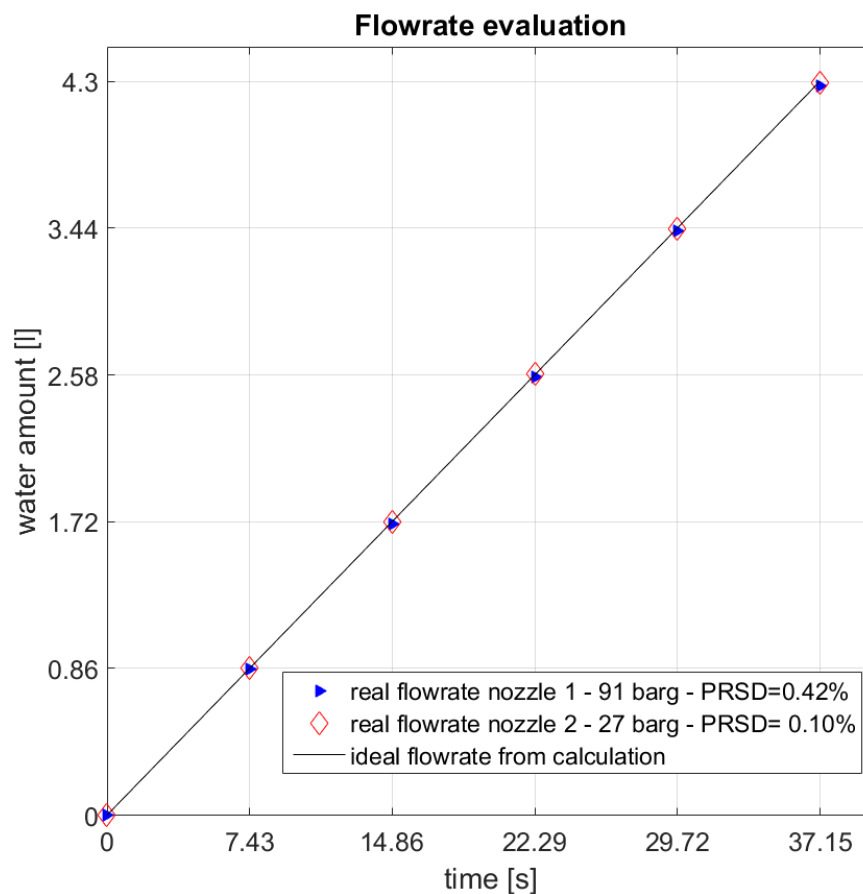


Figure 13 Flowrate evaluation for the two nozzles

### 3.2.4 Experiments implementation

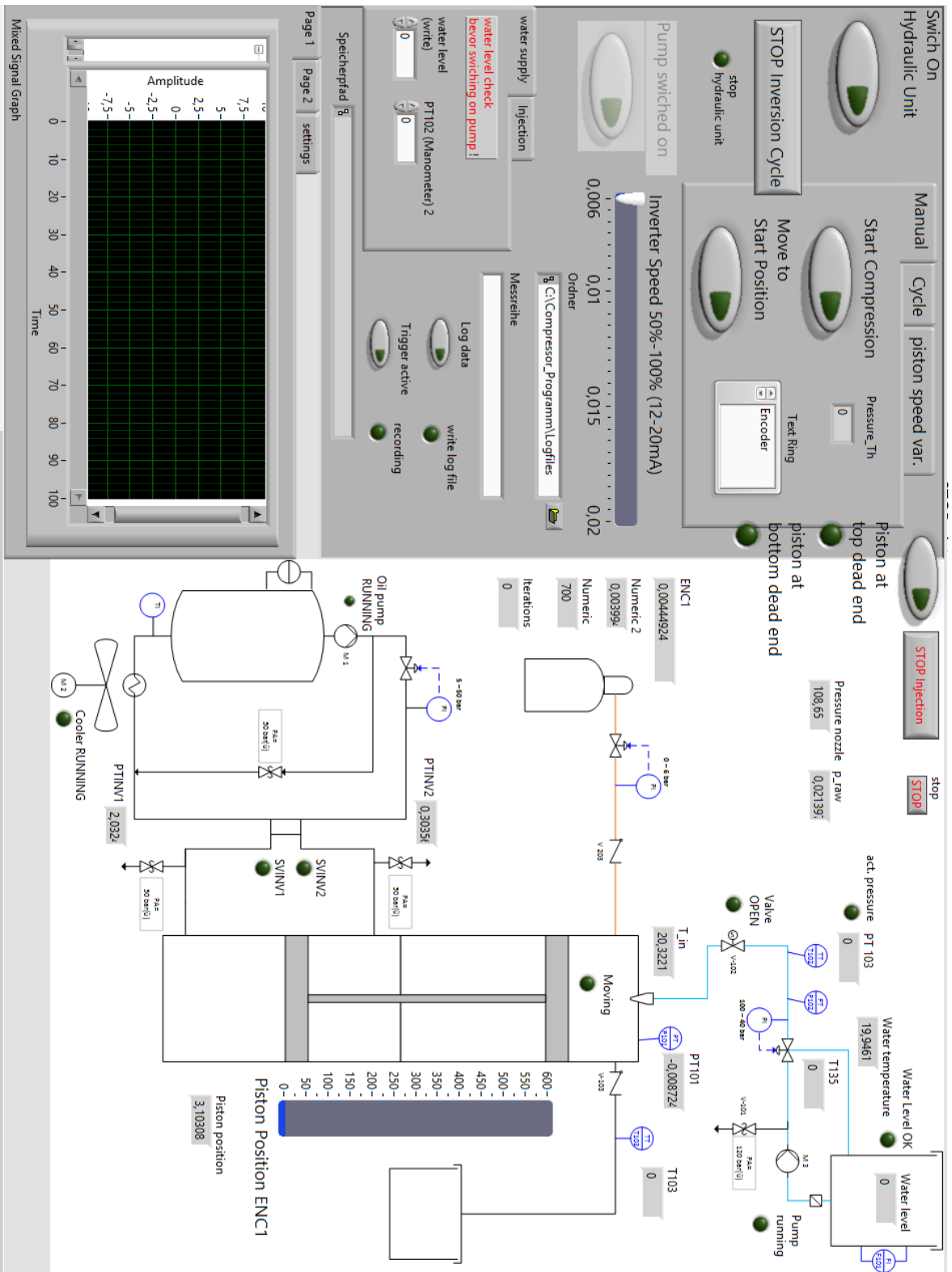
Once that all the parameters of the experiments are chosen, it is possible to start the dissolution process. As already introduced, 4 cases will be performed using two speed configurations and two different nozzles. The aim is to see at the end the effect on the dissolution process and so on the work compression saving for each of the cases just described.

In Picture 10 the LABVIEW control window from where it is possible to control the whole process is presented.

From the left grey box is possible to:

- Switch on and off the hydraulic system
- Vary the initial inverter speed of the hydraulic system and so of the piston
- Set the injection time (opening time of the magnetic valve)
- Set the delay time (positive or negative time slip between compression and injection)
- Set the injection mode:
  - Manual: the user can decide to start injection and compression not simultaneously
  - Automatic: injection and compression start together and their eventually time slip comes from the delay set.
- Start the compression
- Move back the piston to the initial position
- Decide the eventual encoder position or pressure value where I want to stop compression
- Save the data of the compression in a text file in the desired folder.

In the left white box it is possible to see a scheme of the whole test rig with values of the sensors which gives information about the system state: valve position (light on or off), piston position or if it is at the top or dead end.



Picture 10 LABVIEW Control window

For each performed case, it was decided to take 5 experiments in order to make the calculations over the mean of this 5 experiments. In the next subchapter an analysis on the error of this measurement is developed.

### 3.3 Data gathering and filtering method

In this paragraph, the main steps followed in order to calculate the acquired data are presented. In particular, to evaluate average, relative standard deviation and work of each measurement. In order to reduce the error of each measurement, in the LabVIEW code the data were acquired with a frequency of 100. In this way each data is saved 100 times in a second. This can reduce the error of measurement but causes problems of data ordering. This effect comes from the error of the measurement instrument and can be observed in Figure 14.

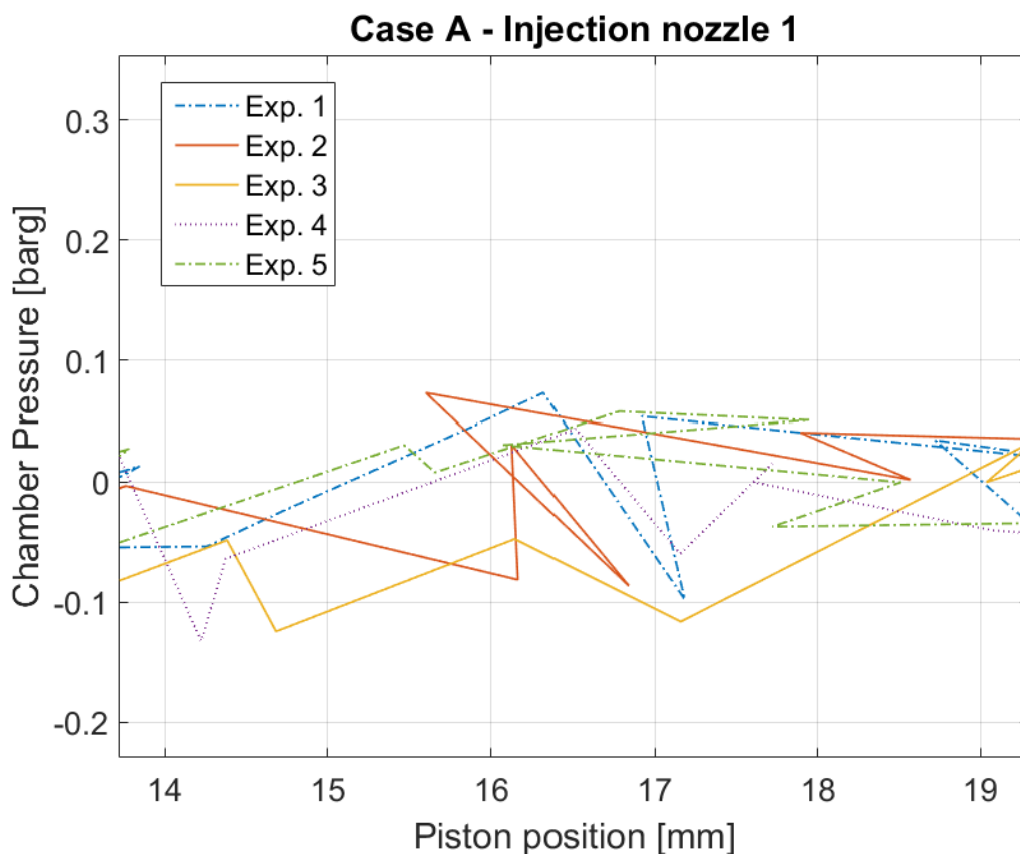


Figure 14 measurement noise

From the same figure it is also visible that since every value of the position vector depends on time, it is not possible to make calculations among the different curves. To allow performing calculations it is needed to have a common position vector for all of the curves. Each value of pressure needs to be evaluated for a new position vector, this is done approximating each curve with a function. The

first attempt was fit each curve using the implemented in Matlab function “fit (x,y,'exp2’). It returns a function of kind  $y = ae^{bx} + ce^{dx}$  built in order to minimize the error defined as the sum of the least square according to equation 3.8

$$error = \sum_{i=1}^n (y_{exponential}(i) - y_{real}(i))^2 \quad (3.8)$$

Where  $y_{exponential}$  represents the fitted function and  $y_{real}$  the experimental data.

Adopting this method, as it is showed in Figure 15 is obtained a not satisfying result. For this reason, it was decided to move towards a filtering method in order to reduce the measurement noise.

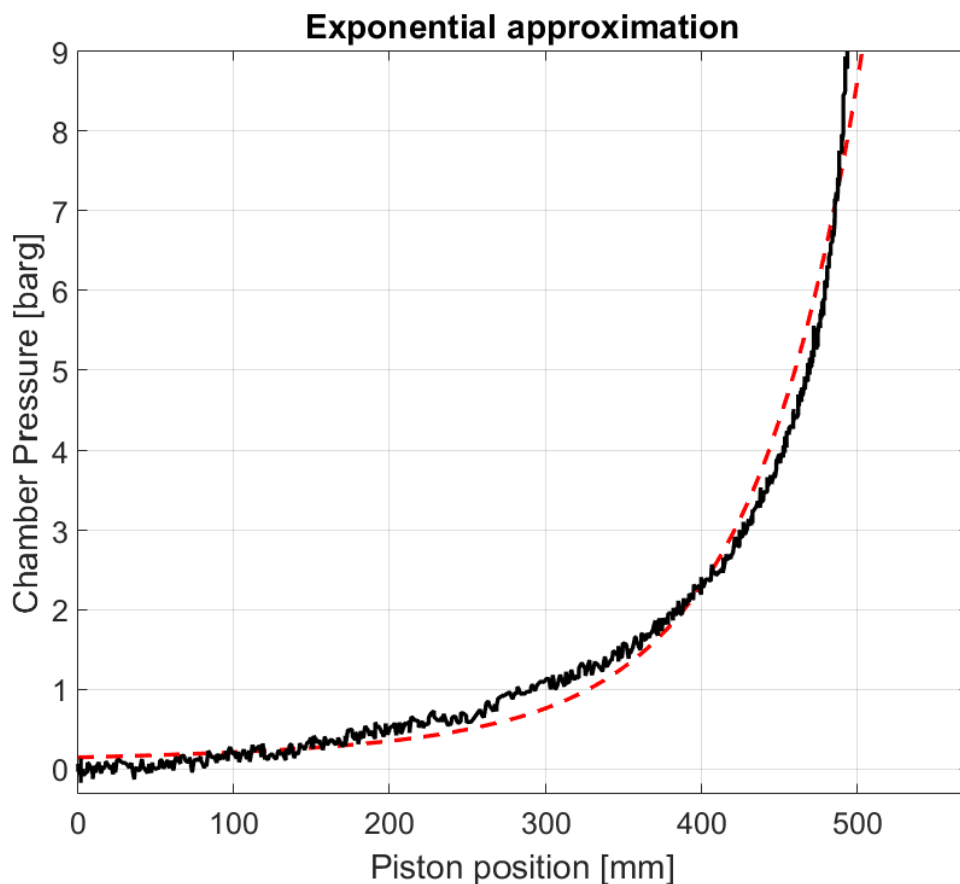


Figure 15 Exponential approximation of experimental data for case B nozzle 1

The second attempt was to use the implemented MATLAB function “Smooth” to reduce the noise and after this to apply an interpolating approximation to obtain a function for every position vector.

The “Smooth” function allows to reduce the noise using several different methods that will be now briefly introduced:

- **Moving average filter** [24]

This filtering method is described by equation 3.9

$$y_{filtered}(i) = \frac{\sum_{i-k}^{i+k} y(i)}{2(k-1) + 1} \quad (3.9)$$

$y_{filtered}$  represents the new fitted value while,  $y(i)$  the real one affected by the measurement noise,  $k$  is the span number, as can be seen from equation 3.9 it describes how many values are involved in the calculation, for higher  $k$  value the smooth effect will be improved but some information about the original experimental curve trend could be lost.

- **LOESS LOWESS** [25]

LOESS LOWESS stands for “locally weighted scatter plot smooth”. Both of these methods use locally weighted linear regression to smooth data. They are described by the following formula:

$$y_{filtered}(i) = \sum_{i-k}^{i+k} w(x)y(i) \quad (3.10)$$

The weight function  $w(x)$  gives different importance to each point according to its relative position with the value where the calculation is centred. The way in which  $w(x)$  is calculated characterizes the accuracy and the computational cost of the method. In particular, when  $w(x)$  is equal to 1 (polynom of zero degree) the method becomes the moving average discussed above. In the Lowess method, the weight function is described by a polynomial of 1 degree that allows us to give more importance on the nearer element in respect to the farther ones in a linear way. As far as the Loess method, the only difference is that the polynomial has a two degree order.

- **Savitzky-Golay Filtering** [26]

This method can be considered as the previous ones with the difference that, the filter coefficients are evaluated with a polynomial with order higher than two. This usually allows to reach a better smoothing effect using low span numbers. Actually, the quality of the filter effect depends on the

initial data pattern. It is not easy to say which method is the best. The choice of the span number comes from a trade-off between filter effect and distance from the experimental data. In order to avoid a too big removal from the experimental data it was decided to evaluate the sum of the least square for the different filtering methods.

As it is possible to see in Figure 16 the error of the pressure sensor is estimated to be  $\leq |0.1|$ .

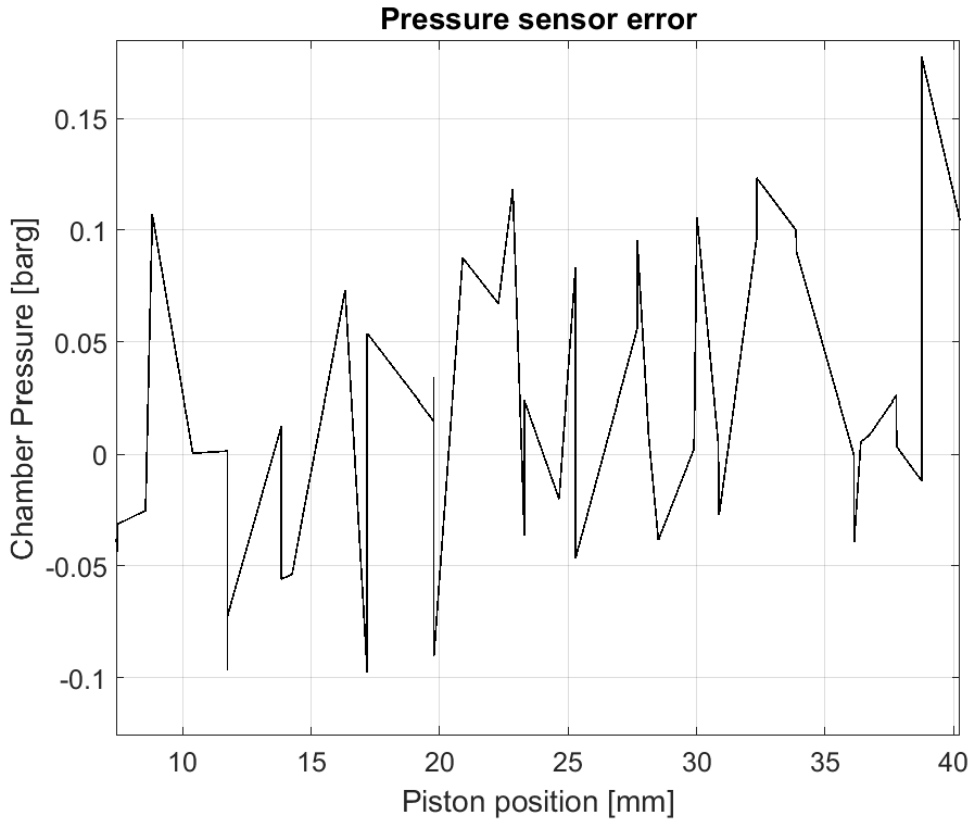


Figure 16 Pressure sensor error, zoom at beginning of compression

At this point, the sum of the least square is calculated according to equation 3.11 for the different filtering methods already described

$$error = \sum_{i=1}^n (y_{filtered}(i) - y(i))^2 \quad (3.11)$$

Taking as example Nozzle A case 1, the error is evaluated over the 1151 elements of the vector using the error of the pressure sensor according to equation 3.12

(3.12)

$$error = \sum_{i=1}^{1151} 0.1^2 = 11.51$$

This value gives information to understand until which span number, the filter method stops to reduce the measurement noise and starts to create a removal from the original data pattern. Every method previously described, has different characteristics and its use depends on the data feature. In order to understand which method gives a better result, the easiest way is to evaluate the error according to equation 3.12 varying the span number  $k$ ; the result is showed in Figure 17.

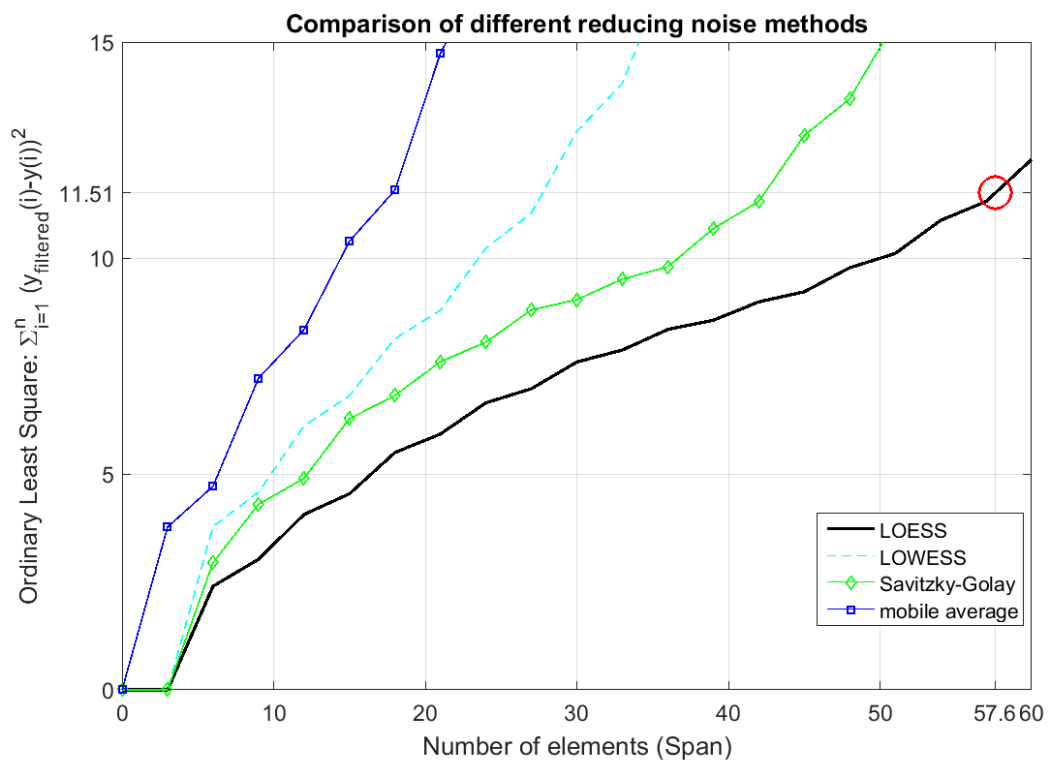


Figure 17 Comparison of different reduction noise method varying the Span number

From Figure 17 it is possible to see that for this data pattern for a bigger span number the Loess method is the one that keeps lower the error. As a result, all the curves will be fitted with Loess method with span number equal to 57.

At this point, still the need to have each curve for a fixed position is present. To solve this problem the filtered curve is approximated with an interpolating linear curve through the implemented MATLAB function "interp1 (x1, y1, x)". This function returns a vector where each element is evaluated according to the new vector x through a linear interpolation applied on the initial curve.

In this way it is possible to describe each curve with a defined common and equidistant new position vector  $x$ . Once these steps are performed, it is possible to approximate each experimental curve with a fitted one as it is showed in Figure 18, the whole procedure is provided in the MATLAB code in appendix.

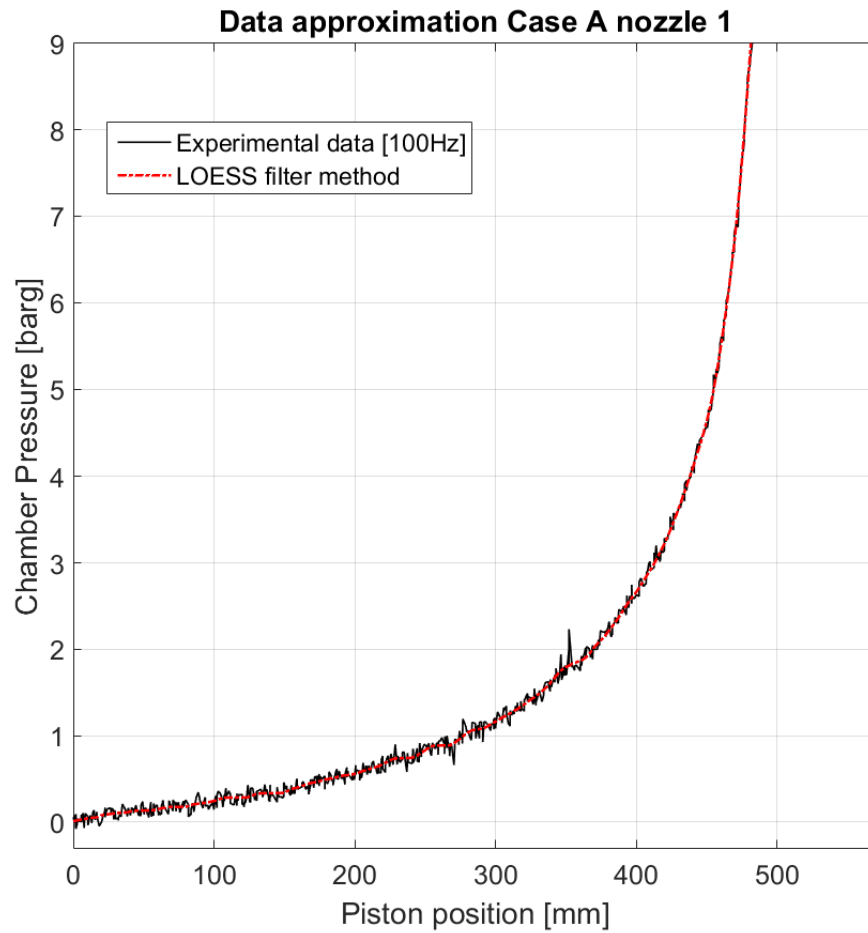


Figure 18 Case A nozzle 1 approximation of the first experiment

The result of the procedure above now allows us to make calculations from the five experimental curves performed for each case. In particular, the average curve and its relative standard deviation are calculated respectively from equation 3.13 and 3.14

$$y_{average} = \frac{\sum_{k=1}^5 y_k}{5} \quad (3.13)$$

$$RSD = \frac{\sqrt{\frac{\sum_{k=1}^5 (y_k - y_{average})^2}{5}}}{|y_{average}|} \quad (3.14)$$

Where  $y_{average}$  is the resultant average curve and  $y_k$  is the  $k^{\circ}$  curve obtained after filtering and interpolation procedure applied on the initial data.

Looking at equation 3.14, because of  $|y_{average}|$  at the denominator all the calculations were done using the absolute pressure. In this way, the evaluation of RSD singularity at the beginning of the compression (relative pressure near to zero) is avoided. The results from case A nozzle 1 are showed in

Figure 19 and in Figure 20 while all the results for all the other cases are provided in Appendix.

Taking into account all the difficulties encountered in order to keep constant the external parameters of the experiments, (e.g. temperature of inlet water, gas temperature in the chamber, different dynamic system response) a PRSD lower than 1.5 % appears a good result.

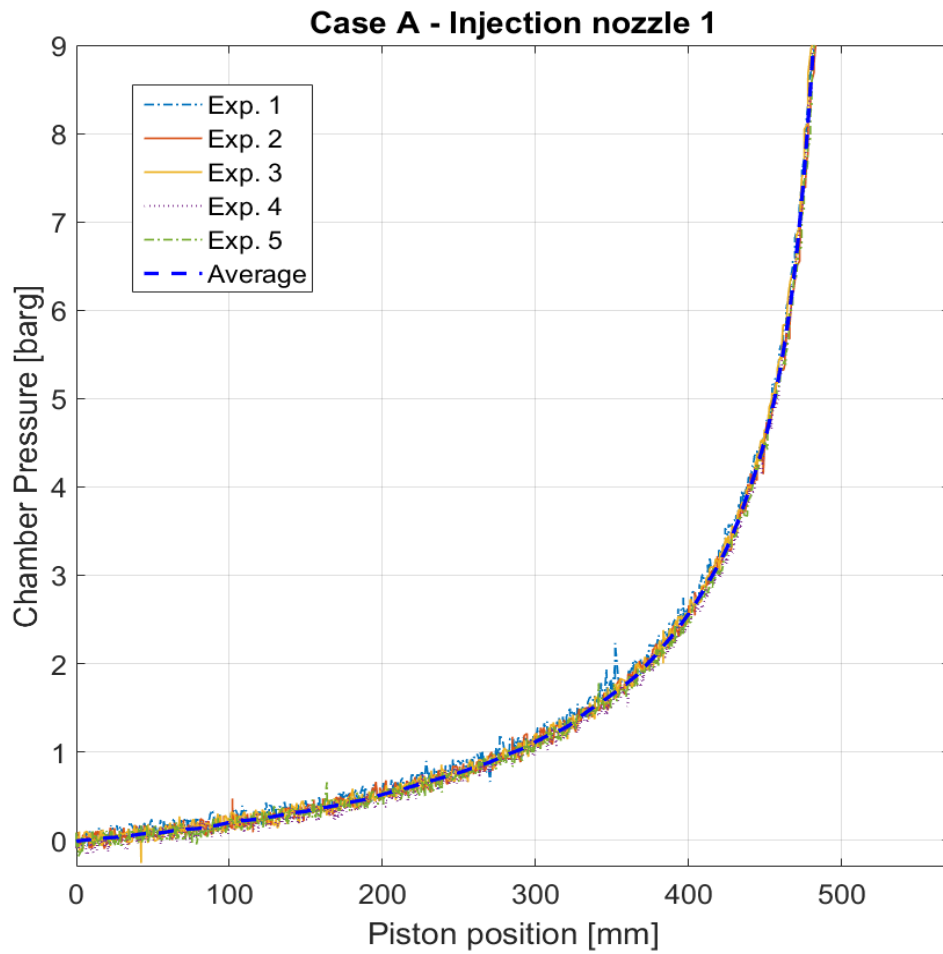
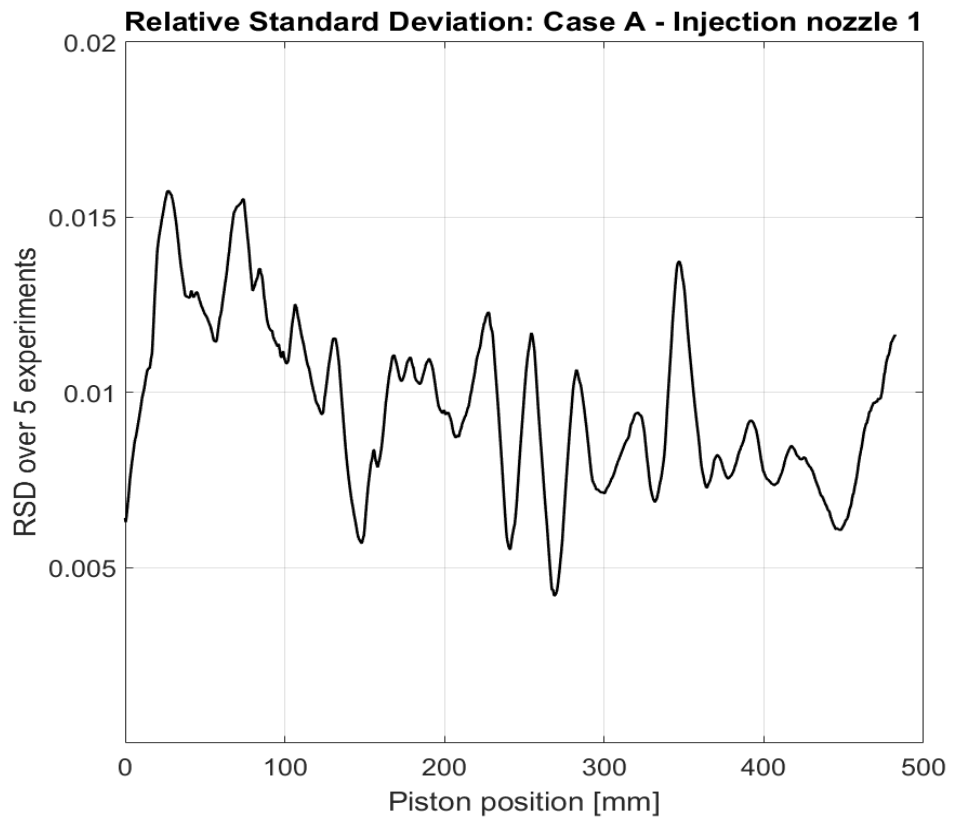


Figure 19 Average curve with raw data of Case A nozzle 1



*Figure 20 RSD over 5 experiments of case A nozzle 1*

## 4 Results

In this chapter the main outcome of the performed experiments are presented. Mainly, attention is given to the comparison of the results with some reference cases. The goal is to show how the speed of the piston and the different momentum of the injection affects the dissolution process in terms of efficiency and work saving. These results provide information on how to proceed in further experiments in order to improve the energy saving.

### 4.1 Outcomes for different nozzle and speed profile

In order to allow an easier reading of the result the main parameters of the experiments are provided in Table 8. The characteristics of the speed for case A and B and all the other used parameters can be found in Chapter 3.2

*Table 8 resume of experiment parameters*

$T_{water} [^{\circ} C]$	25
$T_{CO_2} [^{\circ} C]$	21
$P_{initial} [bar]$	1.02
$P_{final} [bar]$	10
$V_{water} [l]$	0.8603
$P_{nozzle1} [barg]$	91
$P_{nozzle2} [barg]$	27
$t_{inj} [s]$	7.43
$\dot{q} [l/min]$	6.94

In Figure 21 for the four cases already mentioned, the results of the compression are presented. It is possible to appreciate the different influence of dissolution using different nozzles and injection pressure.

It is possible to appreciate how the use of different nozzles and pressure influence the dissolution process for a fixed speed configuration.

It is so possible to observe that the difference of dissolution using different nozzles is more evident in the case of constant speed than in the case of variable speed in which more time is available in the last phase of compression.

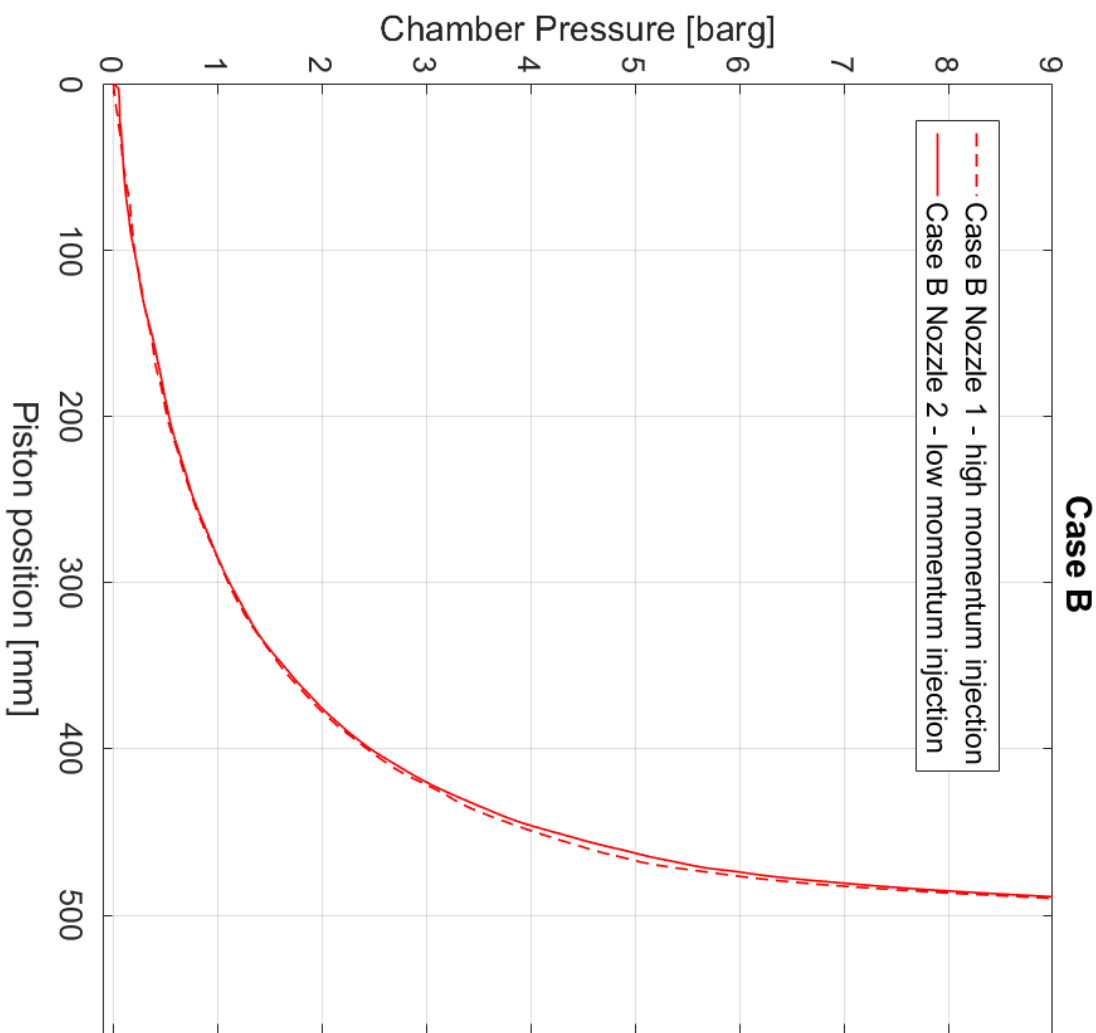
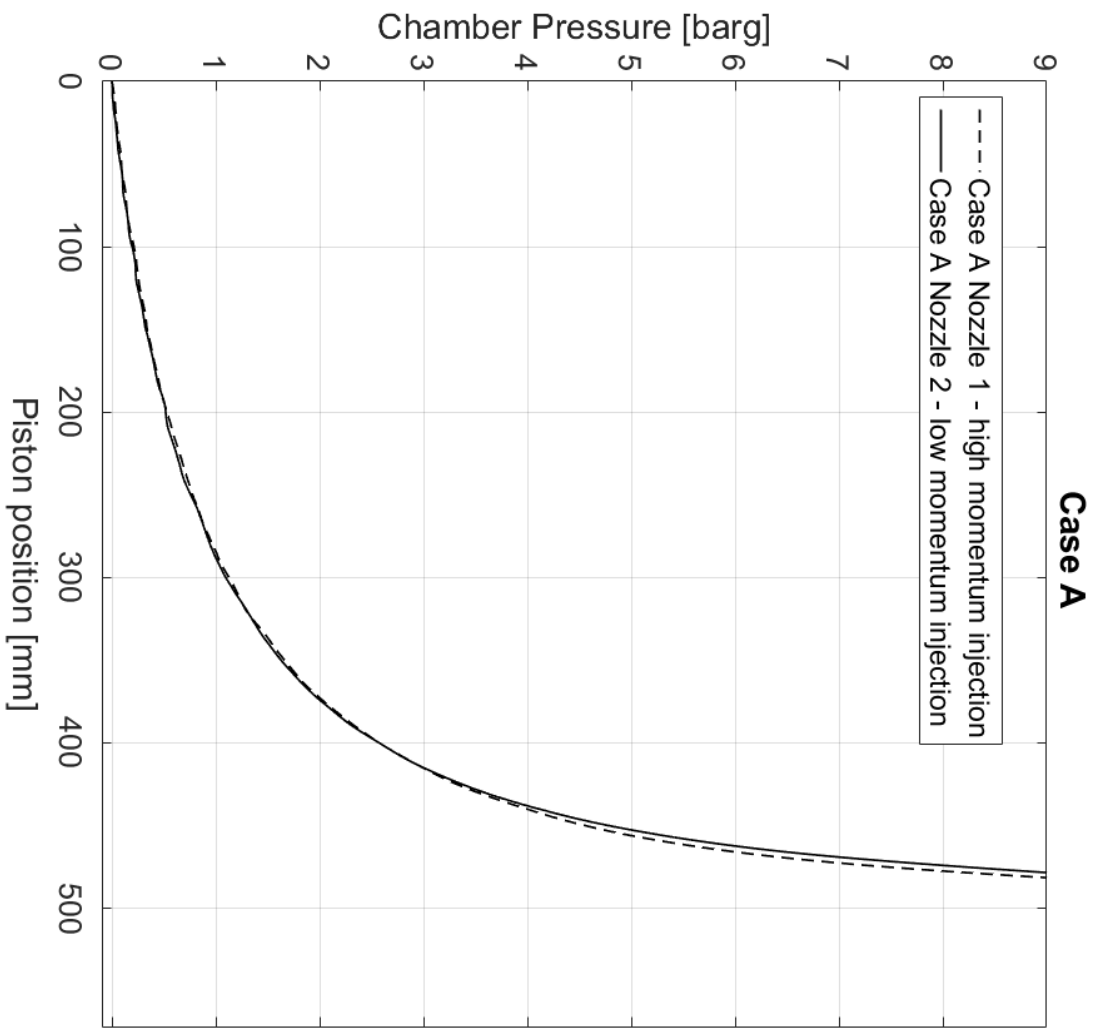


Figure 21 Case A and case B comparison, Injection nozzle 1 and nozzle 2

## 4.2 Reference cases

In order to understand and compare the energy saving of this process, it is useful to define some reference cases and the efficiency related to them. The results above will be compared with:

### 1. Isentropic compression

In order to build the pressure curve for the isentropic compression, a reversible adiabatic transformation was considered [27] according to:

$$P(h) = P_{in} \cdot \left( \frac{V_{in}}{V(h)} \right)^\gamma \quad (4.1)$$

Where:

$P(h)$  is the pressure,  $V(h)$  the chamber volume, both in function of the piston height,  $V_{in}$  is the initial chamber volume,  $P_{in}$  the initial pressure in the chamber,  $\gamma$  is the ratio between constant pressure and volume heat capacity.

### 2. Ideal dissolution process

In order to understand how far is the experimental result from the best case that could be ideally reached, it is needed to define a limit case that is achieved with the following assumptions:

- **Saturation at any time**

This assumption means that at each step the maximum dissolution according to the Henry's law is reached, meaning every time the pressure increases, a steady behaviour is immediately achieved.

- **Isothermal conditions**

Continuous injection is used, this means that it is possible to consider a constant temperature in the process. This is due to the much higher specific heat capacity of water in respect to CO<sub>2</sub> one.

It is reasonable to consider CO<sub>2</sub> as ideal gas [28] because of the range of temperature and pressure used in the compression process. From the ideal gas equation and according to the stated hypothesis, the pressure in function of the piston height can be evaluated according to equation 4.2

$$P(h)_{ideal} = \frac{(n_{CO_2}^0 - k_H p(h)_{ideal} \cdot V_{H_2O}(h)) \cdot R \cdot T_{in}}{A \cdot (h_{stroke} - h) - V_{H_2O}(h)} \quad (4.2)$$

Where:

$n_{CO_2}^0$  is the initial amount of CO<sub>2</sub> in moles in the chamber,  $h_{stroke}$  is the piston stroke,  $R$  the ideal gas constant,  $T_0$  initial chamber temperature,  $V_{H_2O}(h)$  the water volume depending on the piston height (constant flowrate) and  $k_H$  the Henry constant. The term  $k_H p(h)_{ideal} \cdot V_{H_2O}(h)$  represents the moles of CO<sub>2</sub> dissolved in water when the  $P(h)_{ideal}$  is reached. This formula needs an iterative approach to be solved and in order to evaluate this curve in MATLAB, the frozen coefficient method [29] was decided to be implemented. This means that each element of the function  $f$  is evaluated through its previous value (a first attempt value as to be set) as showed in equation 4.3

$$f(i) = g(f(i)) \Rightarrow f(i) = g(f(i-1)) \quad (4.3)$$

This method allows us to avoid the iterative approach and is justified for small change of pressure value. For this reason, in MATLAB the number of elements of the ideal curve was increased from 2  $10^3$  to  $10^5$ .

In Table 9 are provided the parameters used in order to calculate these two reference cases.

*Table 9 Parameter for reference cases evaluation*

$T_{in} [^{\circ} C]$	21
$V_{in} [l]$	7.01
$P_{in} [bar]$	1.02
$h_{stroke} [mm]$	571.5
$k_H [mol \cdot kg^{-1} \cdot bar^{-1}]$	0.034
$n_{CO_2}^0 [mol]$	0.292
$\gamma$	1.29

For each curve, after the piston reaches the encoder position in which 9 barg are achieved, ideally a constant pressure is expected during the expulsion phase. This construction is visible in Figure 22 where the results for case A and B together with the reference cases just described are presented.

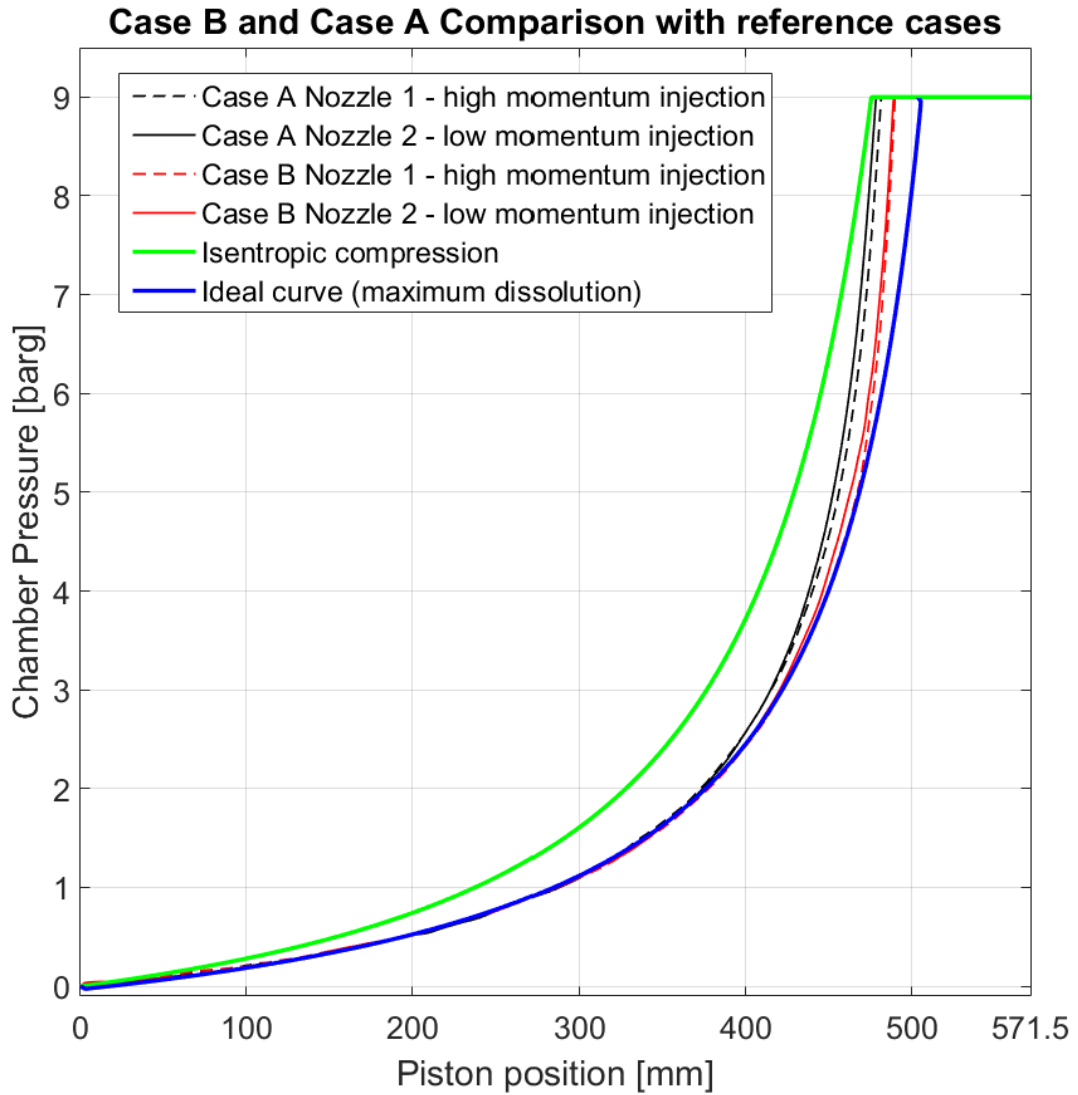


Figure 22 A and B case comparison with reference cases

It is fundamental to remember that because of warming effect from the pump, it was not possible to keep absolutely constant the temperature but was possible to keep the nominal temperature value with an error of  $\pm 0.5$  °C.

### 4.3 Work estimation

From these curves it is possible to observe the results of the several performed experiments but in order to compare them, the spent work in every case is needed to be evaluated. The work for each curve and so the integral value were calculated in MATLAB according to the trapezoidal rule in equation 4.5

$$\int_a^b f(x) = \frac{f(a) + f(b)}{2} \cdot (b - a) \quad (4.5)$$

Where:

$a, b$  are the boundaries of the integral,  $f$  correspond to the pressure that has to be integrated over the height ( $x$ ).

It was needed to decide a way in order to compare the different curves among them using the same conditions. It is not possible to calculate the integral just between 0 and the encoder position in which 9 barg are achieved since this position is located at a different encoder position for every curve. In order to compare the works among them in a proper way, they will be calculated at the same useful effect, follows that in case of compression without injection (isentropic case) has to be taken into account the work needed to compress the same amount of water used in the other case with injection till the pressure of 9 barg.

For the experimental cases and ideal dissolution case the compression works are calculated according to equation 4.6

$$Work_{compression} = Area \int_0^{stroke} p(x) dx \quad (4.6)$$

While for the isentropic compression according to equation 4.7

$$(4.7)$$

$$Work_{compression} = Area \int_0^{stroke} p(x)dx + V_{water}\Delta P$$

Where:

*Area* is the base area of the cylinder, *x* the encoder position, *p(x)* the chamber pressure depending on the encoder position, *V<sub>water</sub>* the amount of injected water that has to be the same in the experimental and ideal case and  $\Delta P$  the pressure variation. The results of the works evaluation is provided in Figure 23.

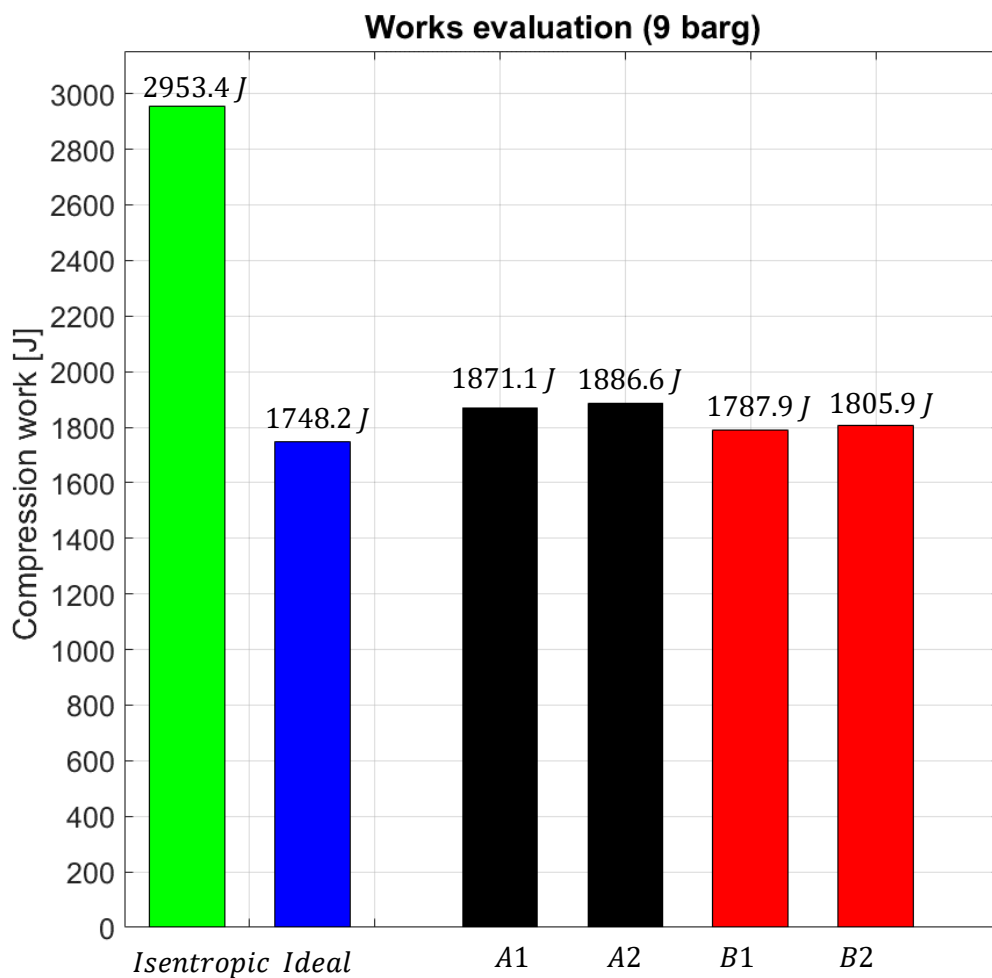


Figure 23 Works evaluation (9barg) Efficiency estimation

In order to have a better idea of the quality of the process, it is possible to define a dissolution efficiency referred to the energy saving obtained in respect to the isentropic compression and the ideal dissolution process according to equation 4.8.

$$\eta_{dissolution} = 1 - \frac{W - W_{id}}{W_{is} - W_{id}} \quad (4.8)$$

Where:

$W$  is the work of the experimental curve,  $W_{id}$  and  $W_{is}$  are the work evaluated according to the ideal and isentropic case as described above. The dissolution efficiency ( $\eta_{dissolution}$ ) is defined in order to be will be 0% if  $W$  is equal to  $W_{is}$  and 100% if it is equal to  $W_{id}$ . The obtained efficiency for each case is provided in Table 10.

*Table 10 dissolution efficiency*

<b>Case</b>	<b><math>\eta_{dissolution}</math> %</b>
<b>A1</b>	89.8
<b>A2</b>	88.5
<b>B1</b>	96.7
<b>B2</b>	95.2

#### 4.4 CELBICON configuration

Once the dissolution process was investigated for the cases described above, it was decided to make the same for the CELBICON configuration. It was required, for the CELBICON project, to investigate the process using the water amount corresponding to a temperature of 40°C. The water amount is calculated according to this new temperature, as already described in chapter 3.2 (water amount evaluation). The main parameters used for this experiment are provided in Table 11 CELBICON configuration - main parameters Table 11.

Table 11 CELBICON configuration - main parameters

$T_{water} [^{\circ} C]$	25
$T_{CO_2} [^{\circ} C]$	21
$V_{water} [l]$	1.20
$P_{nozzle1} [barg]$	91
$t_{inj} [s]$	10.3
$\dot{q} [l/min]$	6.94

The other parameters are kept the same as in the previous experiment. Modifying the amount of water and the injection time, also the speed profile needs to be changed, the procedure to determine it, is the same already described in chapter 3.2 (piston speed evaluation). The speed profile used in this case is provided in Figure 24.

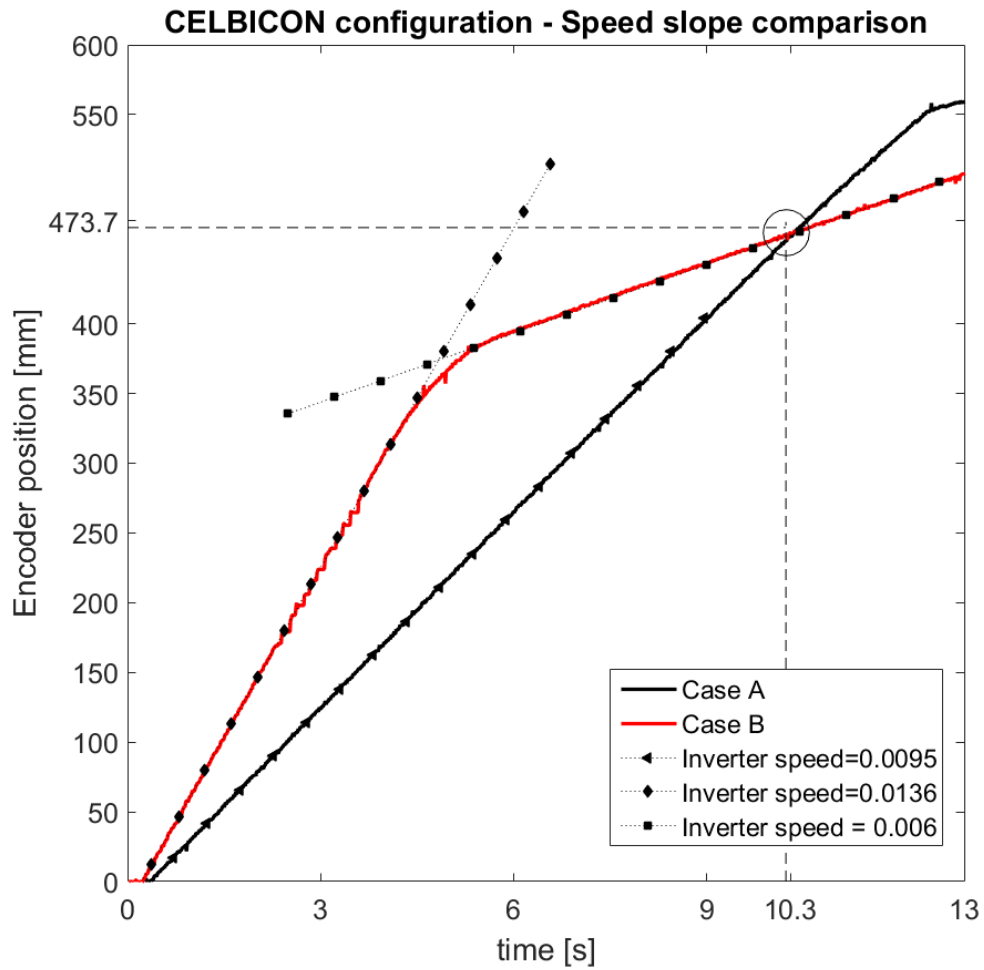


Figure 24 Celbicon conditions - Speed profile comparison

In the new speed profile, it is possible to observe that the encoder position in which the injection ends has decreased since the water column is higher (97.8 mm). This reduction of height doesn't allow us to compare this result with the previous cases. For this reason, in Figure 25 just the new experimental results for case A and B are showed with the reference cases just described above. The ideal dissolution curve is calculated as described above for the new amount of water. It is visible in Figure 25 that it stops at a pressure near to 6 barg. This is the point where the number of CO<sub>2</sub> moles dissolved in the liquid becomes equal to the initial number of moles. This happens because a larger number of gaseous moles dissolves in a larger amount of water for a given pressure. After that point, just the compression of water has to be taken into account.

### Celbicon configuration - Comparison with reference cases

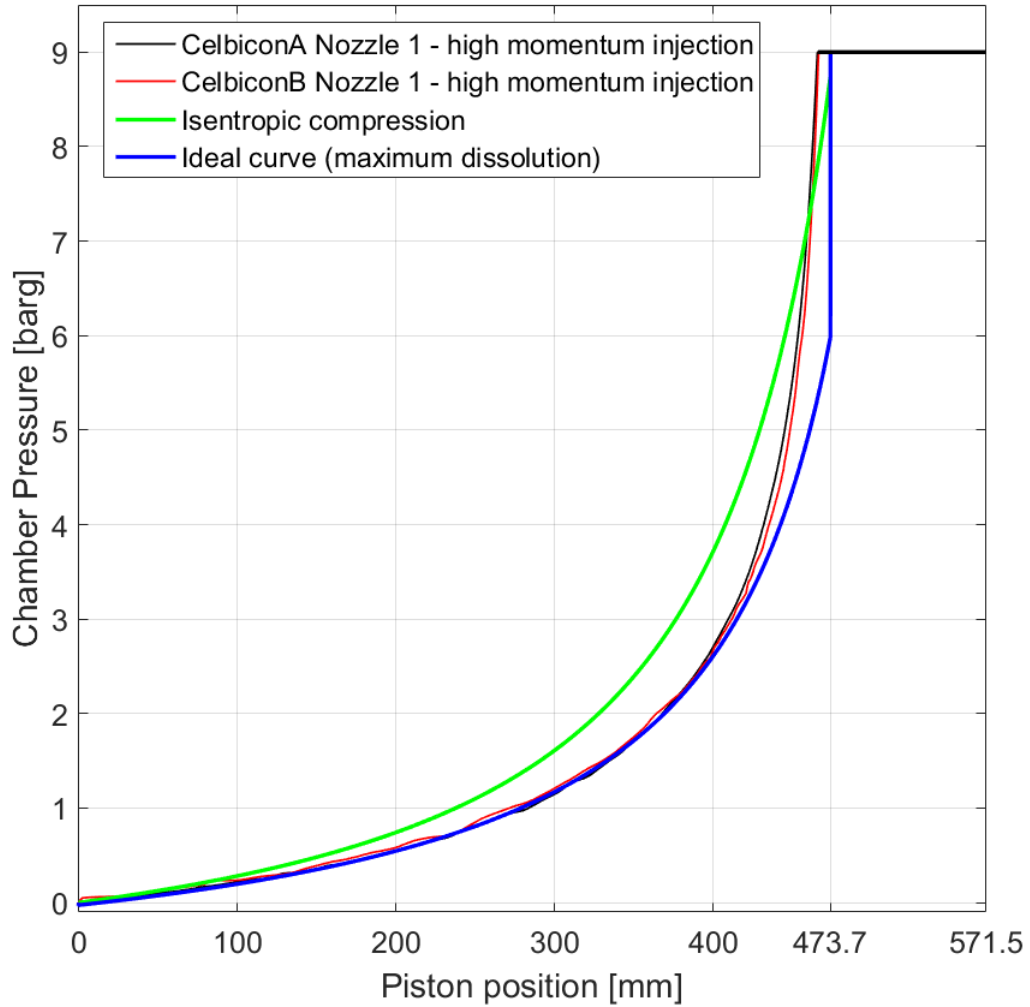
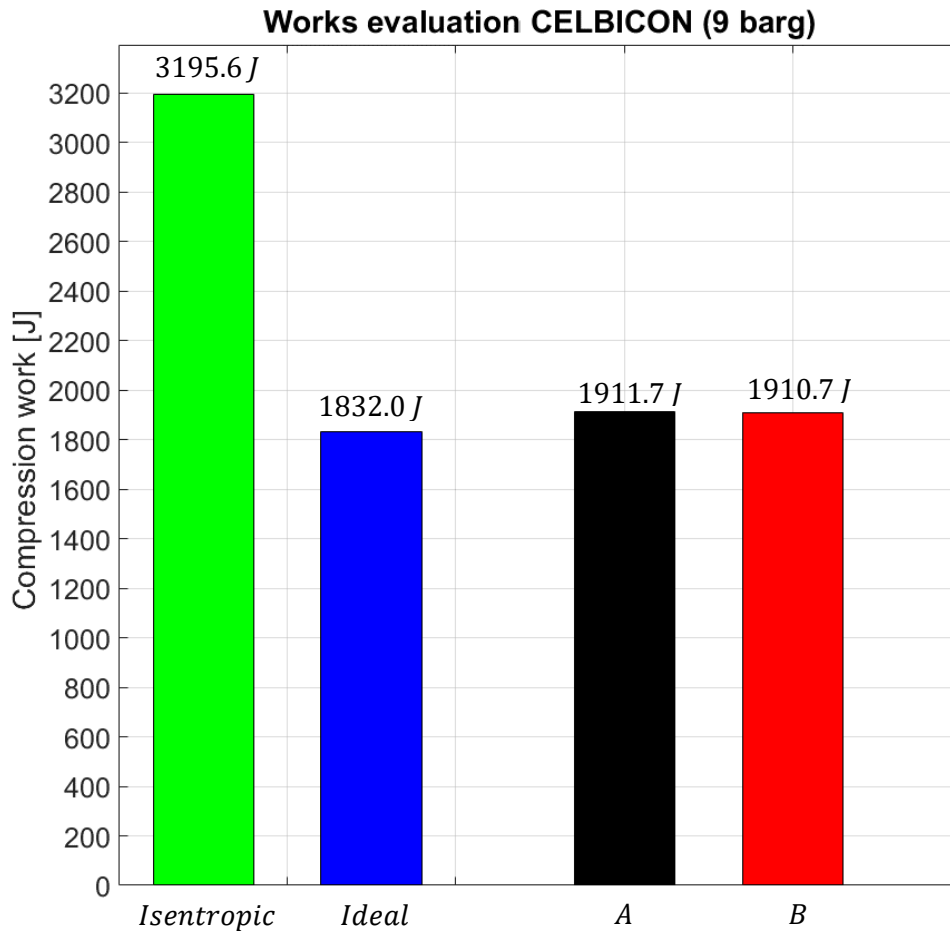


Figure 25 CELCIBON configuration - case A and case B comparison with reference cases

Following the same procedure used above the work is evaluated also for the CELBICON conditions. The results are provided in Figure 26.



*Figure 26 Works evaluation of the CELBICON case*

Also the efficiency as described above is calculated and the result is 94.1% for case A and 94.2% for case B. It is not possible to compare these results with the previous ones because of different parameters involved.

## 5 Conclusions

In this chapter, the final considerations of the entire process will be carried out. Preferential attention is given to possible further investigations for the improvement of the process.

Looking back at the provided results in chapter 4, it is possible to make some observation.

Until the pressure of 2 barg is reached, the different effect in dissolution is not so evident for the 4 different cases; the strong reduction of work respect to the isentropic is probably due to the water spray that allows to have a more isothermal behaviour of compression.

Dissolution for nozzle 1 ( $P_{nozzle1} = 91 \text{ barg}$ ) is enhanced because of higher momentum that enhances the diffusivity process (Fick's Law). The dissolution in this case is enhanced because of higher pressure and so because of smaller diameter and higher speed of the droplets. In addition nozzle 1 has a more narrow angle ( $45^\circ$  instead of  $60^\circ$ ) this allows to reach the piston when it is in a further position in respect to the case with nozzle 2 and so to have a longer turbulence phase.

In case A the faster speed (at least after the 2/3 of the stroke) doesn't allow a good dissolution as in case B, for this reason more  $\text{CO}_2$  moles remain in the gaseous phase, following that when the nozzle 1 is used (better spray pattern) the dissolution improvement is higher in respect to case B in which already more dissolution is allowed by lower compression speed.

The work reduction obtained using a higher injection pressure is much lower than the work reduction obtained just by changing the speed configuration.

From the observation just pointed out, it is possible to list the following outcomes about the process:

- the importance of slowing down the speed increases for growing pressure;
- Injection is needed during all the compression in order to ensure a constant cooling effect;
- It is important to inject especially until the end of the compression because the mass transfer is much more enhanced by the higher gas pressure and turbulence is needed in order to allow a better dissolution and better cooling of the compressed gas;
- High pressure injection does not seem to be really needed, at least for this kind of geometry chamber. It could be needed most in case of higher piston speed.
- Low speed has to be ensured at least when pressure is higher than 2 barg.

From the CELBICON case is also possible to see that the saving of work due to different speed is neglectable respect to the previous case, this is due to the already better dissolution given by the much longer injection time.

Taking into account all the provided results, and the sequent considerations, with this chamber geometry it seems reasonable to take in consideration the idea to substitute the full cone nozzle typology, with a free injection one. This solution comes from the consideration that most of the surface energy to atomize the spray is lost because of subsequent coalescence of the spray at the cylinder wall and because of internal swirling. Using a free injection nozzle, all the pressure energy is converted in momentum, the swirling effect starts from the beginning of the compression because of longer distance reached with this kind of injection.

It could be also taken into account the idea to modify the piston crown, in correspondence to the point in which the free jet impacts by installing a tool that enhances turbulence in the chamber. Alternatively, the use of a full cone nozzle could be tested with a new chamber geometry. Another idea could be also the same chamber but horizontal instead of vertical. In this way it is possible to use nozzles with wider angle that ensures a finer atomization with less coalescence at the chamber wall and most important previous start of swirling occurrence.

Apart the observation just proposed would be also of great interest to create a database in which the energy saving is recorded for different dissolution time in order to provide a tool that could help to size this kind of compressors depending on the required yield. In this way, the choice of the size will come from a trade-off between investment (piston size) and operating (energy saving) costs.

It would be interesting also to understand which one is the component of the isothermal effect respect to the dissolution one, in terms of work reduction. To do this is needed to know how the temperature of the gas evolves during the compression, this can be done using a much faster thermocouple.

In order to understand in a proper way how the whole process evolves, is fundamental to investigate also inside the spray in order to know the real size and the speed of the droplets and also how the coagulation and the swirling effect develops.

## 6 References

- [1] Europe commission clima policies, [Online]. Available: [https://ec.europa.eu/clima/policies/international/negotiations/paris\\_en](https://ec.europa.eu/clima/policies/international/negotiations/paris_en).
- [2] IPCC, "Fifth Assessment Report of the Intergovernmental Panel on Climate Change," 2014.
- [3] E. Wolf, "Large-Scale Hydrogen Energy Storage," *Elsevier*, pp. 129-142, 2015.
- [4] Celbicon Project, "Project summary, Celbicon," [Online]. Available: <http://www.celbicon.org/>.
- [5] W. Henry, Experiments on the quantity of gases absorbed by water, at different temperatures, and under different pressure, London, 1803.
- [6] R. Sander, Compilation of Henry's law constants (v4.0) for water as solvent ( vol.15 pp4399-4981), 2015.
- [7] N. N. Greenwood and A. (. Earnshaw, "Chemistry of the Elements (2nd ed.)," *Butterworth-Heinemann*, p. 310.
- [8] R. R. A.Cavaliere, "Atomizzazione Capitolo 5".
- [9] L. Arthur H, "Properties of Sprays, paper for International Conference on Mechanics of Two-Phase Flows, Tapei Taiwan," *Particle*, vol. 6, pp. 176-186, (1989).
- [10] K. P. Stephen W. Webb, "The use of Fick's Law for Modeling Trace Gas Diffusion in Porous Media," *Springer Link*, vol. 51, pp. 327-341, 2003.
- [11] J. G. I. T. Diego Caratelli, "Spherical Harmonic Solution of the Robin Problem for the Helmholtz Equation in a Supershaped Shell," *Applied Mathematics*, vol. 4, 2012.
- [12] Springer, VDI Heat Atlas Pag.24 Correlation valid with error < 2% for sphere geometry with Fourierier number  $\geq 0.18$ , Biot number  $\rightarrow \infty$  and constant concentration at the surface, Springer, 2010.
- [13] A. M. T.D Eastop, Applied Thermodynamics For Engineering Technologists: Solutions Manual, 1993.
- [14] Università degli studi di Parma, 2014. [Online]. Available: [http://pcfarina.eng.unipr.it/Public/Fisica-Tecnica-2014/Dispense/06\\_Lezione\\_21\\_03\\_14\\_Camisa\\_Fedreghini.pdf](http://pcfarina.eng.unipr.it/Public/Fisica-Tecnica-2014/Dispense/06_Lezione_21_03_14_Camisa_Fedreghini.pdf).

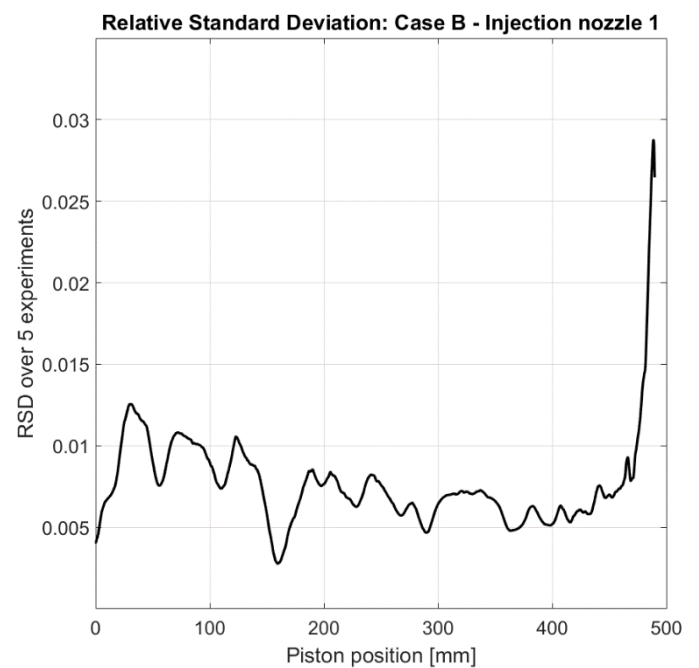
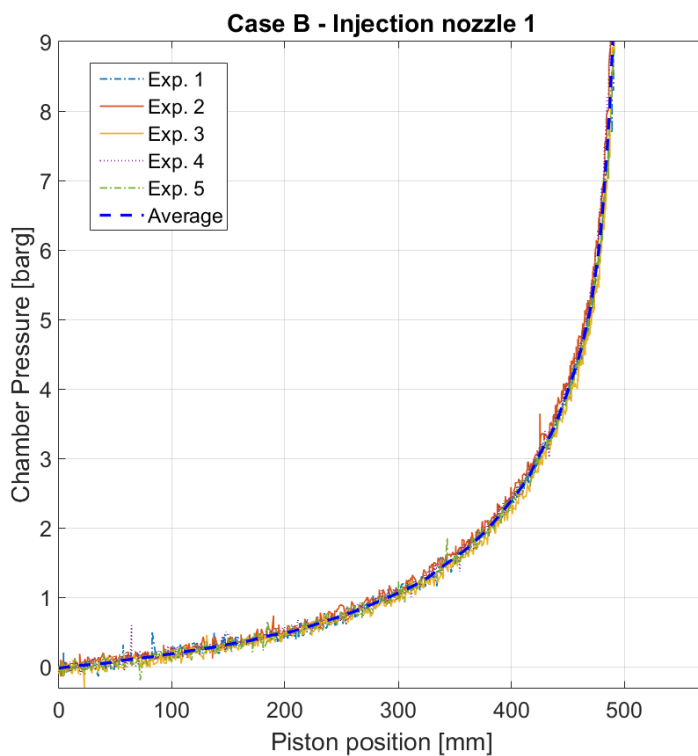
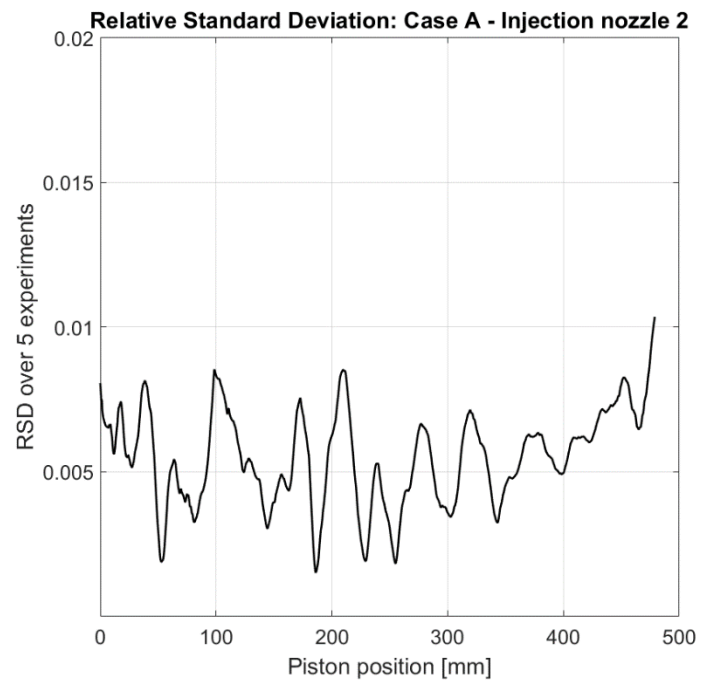
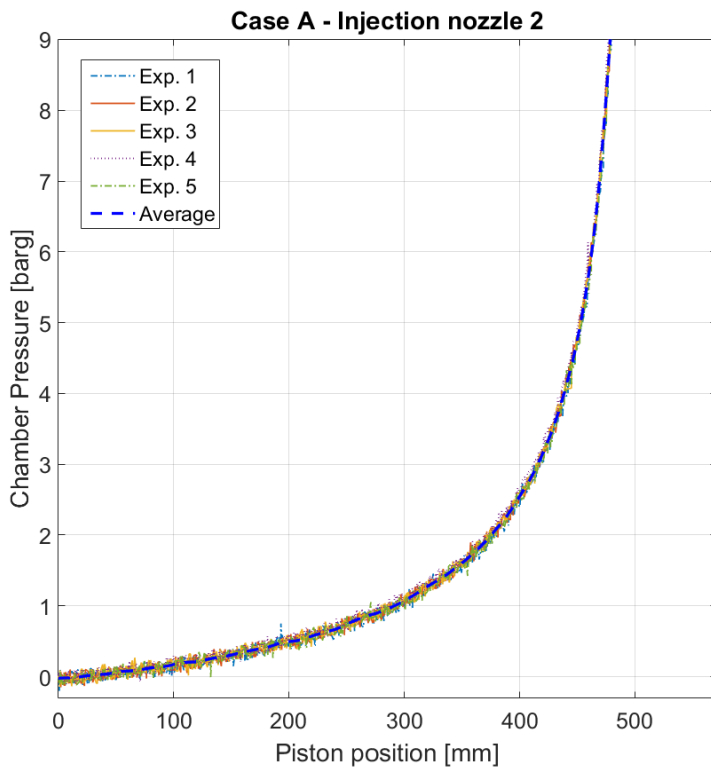
- [15] D. M. a. W. Y. Shiu, "A critical review of Henry's law constants for chemicals of environmental interest," *Journal of Physical and Chemical Reference Data*, vol. 1175, 1981.
- [16] J. D. S. a. A. E. M. John J. Carroll, "The Solubility of Carbon Dioxide in water at Low Pressure," *Journal of Physical and Chemical Reference Data* 20, vol. 1201, 1991.
- [17] Patent US Grant, 4 Jan 1938. [Online]. Available: <https://patentimages.storage.googleapis.com/c1/e2/4e/80142c29a692ac/US2104687.pdf>.
- [18] W. J. Rouleau, "Patent US Grant," 6 May 1947. [Online]. Available: <https://patentimages.storage.googleapis.com/84/f7/bc/9c260b36fd378a/US2420098.pdf>.
- [19] J. L. Eric L. Winandy, "Scroll compressors using gas and liquid injection: experimental analysis and modelling," *ELSEVIER*, vol. 25, no. Issue 8, pp. 1143-1156, 2002.
- [20] MTS sensors, "Magnetostrictive Linear-Position Sensors," [Online]. Available: [https://www.controldesign.com/assets/wp\\_downloads/pdf/mts\\_sensors.pdf](https://www.controldesign.com/assets/wp_downloads/pdf/mts_sensors.pdf).
- [21] Burkert, "Servogesteuerte 2/2 Wege Kolbenventil," [Online]. Available: <https://www.burkert.it/it/type/2400>.
- [22] Virginia State university, "Nozzle selection and sizing," [Online]. Available: [https://pubs.ext.vt.edu/content/dam/pubs\\_ext\\_vt\\_edu/442/442-032/442-032\\_pdf.pdf](https://pubs.ext.vt.edu/content/dam/pubs_ext_vt_edu/442/442-032/442-032_pdf.pdf).
- [23] Lechler, [Online]. Available: [http://www.lechler.in/is-bin/intershop.static/WFS/LechlerIN-Shop-Site/LechlerIN-Shop/en\\_IN/PDF/02\\_produkte/industrie/Brochures/lechler\\_brochure\\_chemicalindustry\\_GB\\_1115\\_mail.pdf](http://www.lechler.in/is-bin/intershop.static/WFS/LechlerIN-Shop-Site/LechlerIN-Shop/en_IN/PDF/02_produkte/industrie/Brochures/lechler_brochure_chemicalindustry_GB_1115_mail.pdf).
- [24] Mathworks, "Mathworks Documentation Moving average filter," [Online]. Available: <https://it.mathworks.com/help/econ/filtering.html>.
- [25] Mathworks, "Mathworks Documentation Filtering and Smoothing Data," [Online]. Available: <https://it.mathworks.com/help/curvefit/smoothing-data.html>.
- [26] MathWorks, "MathWork Documentation Savitzky-Golay Filtering," [Online]. Available: [https://it.mathworks.com/help/curvefit/smoothing-data.html#bq\\_6ys3-2](https://it.mathworks.com/help/curvefit/smoothing-data.html#bq_6ys3-2).
- [27] "Chimicamo," [Online]. Available: <https://www.chimicamo.org/chimica-fisica/trasformazione-adiabatica.html>.
- [28] "Pressure, Volume, and Temperature Relationships in Real Gases," [Online]. Available: [https://chem.libretexts.org/Textbook\\_Maps/General\\_Chemistry/Map%3A\\_Chemistry\\_-](https://chem.libretexts.org/Textbook_Maps/General_Chemistry/Map%3A_Chemistry_-)

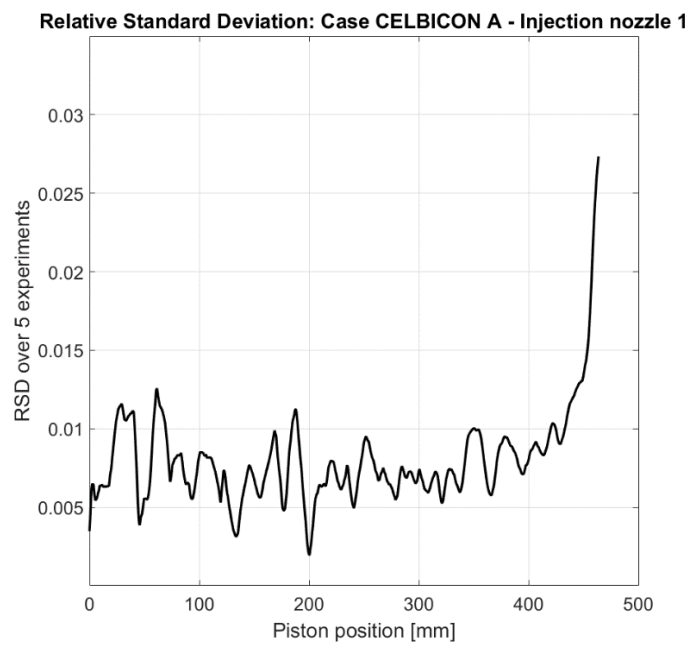
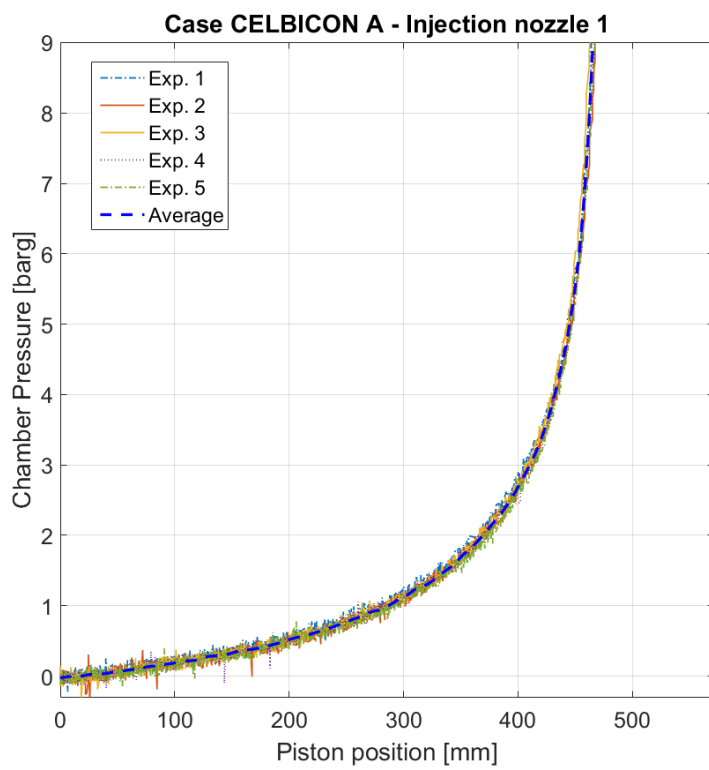
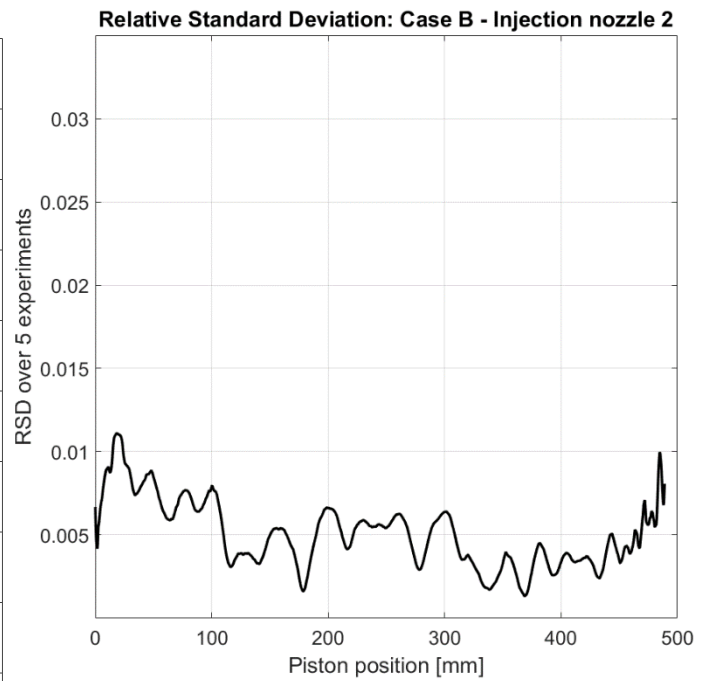
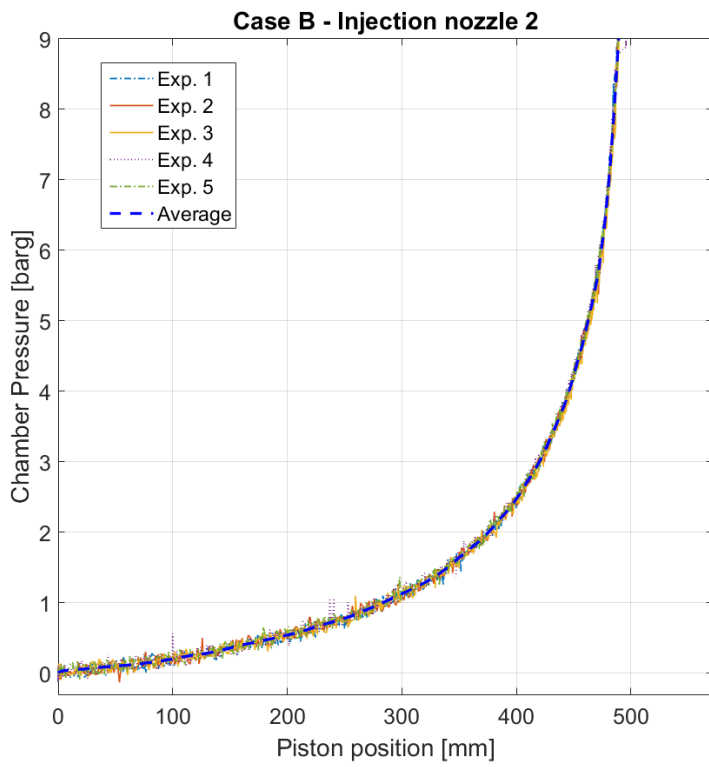
\_The\_Central\_Science\_(Brown\_et\_al.)/10%3A\_Gases/10.9%3A\_Real\_Gases\_-  
\_Deviations\_from\_Ideal\_Behavior.

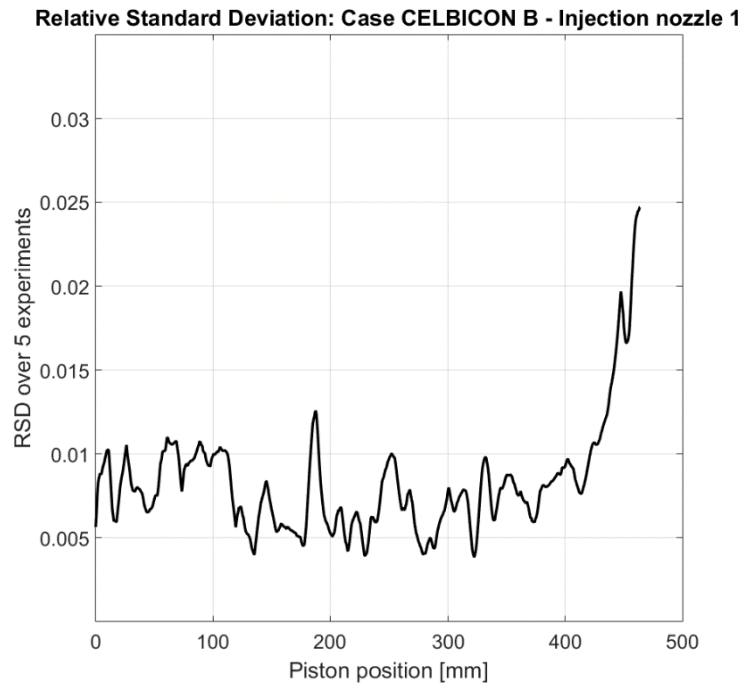
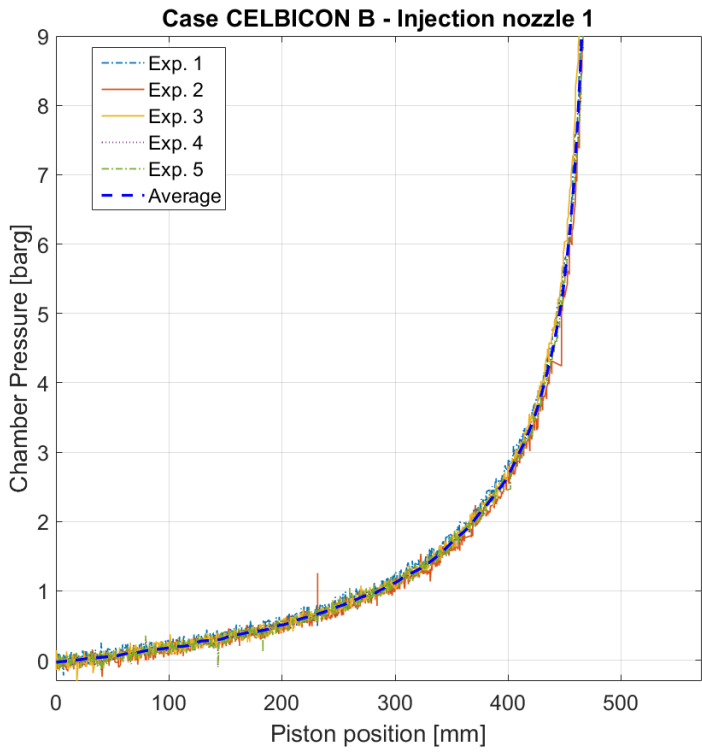
- [29] J. ELavery, "A comparison of the method of frozen coefficients with Newton's method for quasilinear two-point boundary-value problems," *Journal of Mathematical Analysis and Applications*, vol. 123, pp. 415-428, 1987.

## 7 Appendix

In this Chapter are provided the results of the performed experiment, included the CELBICON one, Follows the MATLAB code used for the acquisition, and filtering of the data and finally an example of a txt file where the experimental results are saved form LABVIEW.









```

k(3)=min(find(pressure3>=pressure_th)
);
k(4)=min(find(pressure4>=pressure_th)
);
k(5)=min(find(pressure5>=pressure_th)
);
%
time1=time1-time1(1);% the time from
the txt doesn't start from zero
time2=time2-time2(1);
time3=time3-time3(1);
time4=time4-time4(1);
time5=time5-time5(1);
time1=time1/1000;%second %time was in
milliseconds
time2=time2/1000;%second
time3=time3/1000;%second
time4=time4/1000;%second
time5=time5/1000;%second
% scaling process of the vectors
position1=(position01(1:1:j(1))-
position01(1));
scale=stroke/position1(end);
position1=position1*scale;
pressure1=pressure1(1:1:j(1));
%
position2=(position02(1:1:j(2))-
position02(1));
scale=stroke/position2(end);
position2=position2*scale;
pressure2=pressure2(1:1:j(2));
%
position3=(position03(1:1:j(3))-
position03(1));
scale=stroke/position3(end);
position3=position3*scale;
pressure3=pressure3(1:1:j(3));
%
position4=(position04(1:1:j(4))-
position04(1));
scale=stroke/position4(end);
position4=position4*scale;
pressure4=pressure4(1:1:j(4));
%
position5=(position05(1:1:j(5))-
position05(1));
scale=stroke/position5(end);
position5=position5*scale;
pressure5=pressure5(1:1:j(5));
%
max=max(k);%i need this value in
order to ensure that each vector has
reached 9.0 bar
positionmean=linspace(0,stroke,2000);
%calculation for the work evaluation
%the delta x is different in each
element, because of error of sensor
and
%because pressure increase with
different speed
deltax1=zeros(1,k(1));
for h1=1:k(1)-1
    deltax1(h1)=position1(h1+1)-
position1(h1);
end
deltax2=zeros(1,k(2));
for h2=1:k(2)-1
    deltax2(h2)=position2(h2+1)-
position2(h2);
end
deltax3=zeros(1,k(3));
for h3=1:k(3)-1
    deltax3(h3)=position3(h3+1)-
position3(h3);
end
deltax4=zeros(1,k(4));
for h4=1:k(4)-1
    deltax4(h4)=position4(h4+1)-
position4(h4);
end
deltax5=zeros(1,k(5));
for h5=1:k(5)-1
    deltax5(h5)=position5(h5+1)-
position5(h5);
end
%work calculations
work(1)=workconst*sum(pressure1(1:1:k
(1)).*(deltax1));
work(2)=workconst*sum(pressure2(1:1:k
(2)).*(deltax2));
work(3)=workconst*sum(pressure3(1:1:k
(3)).*(deltax3));
work(4)=workconst*sum(pressure4(1:1:k
(4)).*(deltax4));
work(5)=workconst*sum(pressure5(1:1:k
(5)).*(deltax5));
work
%Joule
%end

%data ordering before the smooth
application
% this operation is needed to apply
the function to smooth below
for i=2:max
    if position1(i)<=position1(i-1)
        position1(i)=position1(i-
1)+0.001;
    end
    if position2(i)<=position2(i-
1)
        position2(i)=position2(i-
1)+0.001;
    end
    if position3(i)<=position3(i-
1)
        position3(i)=position3(i-
1)+0.001;
    end
    if position4(i)<=position4(i-
1)
        position4(i)=position4(i-
1)+0.001;
    end
    if position5(i)<=position5(i-
1)
        position5(i)=position5(i-
1)+0.001;
    end
end
%smooth application using the loess
method and the span number that comes
%from the analysis performed in
Chapter 3 (Data gathering)

```

```

ysmooth1=smooth(position1(1:1:max),pr
essure1(1:1:max),span,'loess');
ysmooth2=smooth(position2(1:1:max),pr
essure2(1:1:max),span,'loess');
ysmooth3=smooth(position3(1:1:max),pr
essure3(1:1:max),span,'loess');
ysmooth4=smooth(position4(1:1:max),pr
essure4(1:1:max),span,'loess');
ysmooth5=smooth(position5(1:1:max),pr
essure5(1:1:max),span,'loess');

%this operation is needed because
could happen that for higher value of
x I
%have lower pressure, and this
doesn't allow to make the
interpolation
%below
for i=2:max
    if ysmooth1(i)<=ysmooth1(i-1)
        ysmooth1(i)=ysmooth1(i-
1)+0.0001;
    end
    if ysmooth2(i)<=ysmooth2(i-1)
        ysmooth2(i)=ysmooth2(i-
1)+0.0001;
    end
    if ysmooth3(i)<=ysmooth3(i-1)
        ysmooth3(i)=ysmooth3(i-
1)+0.0001;
    end
    if ysmooth4(i)<=ysmooth4(i-1)
        ysmooth4(i)=ysmooth4(i-
1)+0.0001;
    end
    if ysmooth5(i)<=ysmooth5(i-1)
        ysmooth5(i)=ysmooth5(i-
1)+0.0001;
    end
end
%interpolation is needed to allow
calculation among the different
vectors.
y1=interp1(position1(1:1:max),ysmooth
1,positionmean);
y2=interp1(position2(1:1:max),ysmooth
2,positionmean);
y3=interp1(position3(1:1:max),ysmooth
3,positionmean);
y4=interp1(position4(1:1:max),ysmooth
4,positionmean);
y5=interp1(position5(1:1:max),ysmooth
5,positionmean);
%application of average and PRSD
for g=1:1:2000
    ymean(g)=(y1(g)+y2(g)+y3(g)+y4(g)+y5(
g)+5)/5;
    ymom2ord(g)=((y1(g)+1)^2+(y2(g)+1)^2+
(y3(g)+1)^2+(y4(g)+1)^2+(y5(g)+1)^2)/
5;
    vari(g)=ymom2ord(g)-ymean(g)^2;
    RSD(g)=sqrt(abs((vari(g)/5)))/(abs(ym
ean(g)));
end
%plot1
figure(1)
hold on
box on
grid on
axis square
orient landscape
set(gca,'FontSize',15);
title('Case B - Injection nozzle 1');
plot(position1(1:1:max),pressure1(1:1
:max),'-
','LineWidth',1,'MarkerEdgeColor',[0
.3 0.6 0.2]);
plot(position2(1:1:max),pressure2(1:1
:max),'-
','LineWidth',1,'MarkerEdgeColor','g'
);
plot(position3(1:1:max),pressure3(1:1
:max),'-
','LineWidth',1,'MarkerEdgeColor',[0.
3 0.6 0.2]);
plot(position4(1:1:max),pressure4(1:1
:max),':','LineWidth',1,'MarkerEdgeCo
lor','g');
plot(position5(1:1:max),pressure5(1:1
:max),'-
','LineWidth',1,'MarkerEdgeColor','g
');
plot(positionmean,(ymean-1),'b--
','linewidth',2);
axis([0 stroke -0.3 9]);
xlabel('Piston position [mm]');
ylabel('Chamber Pressure [barg]');
legend('Exp. 1 ','Exp. 2','Exp.
3','Exp. 4','Exp.
5','Average','SouthEast');
figure(2)
hold on
box on
grid on
axis square
set(gca,'FontSize',15);
plot(position1(1:1:max),pressure1(1:1
:max),'k-','linewidth',1.5);
plot(positionmean,y1,'r--
','linewidth',1.5);
title('Data approximation Case B
nozzle 2')
axis([0 stroke -0.3 9]);
xlabel('Piston position [mm]');
ylabel('Chamber Pressure [barg]');
legend('Experimental data
[100Hz]','LOESS filter
method','Location','SouthEast');
figure(3)
axis square
hold on
box on
set(gca,'FontSize',15);
orient landscape
grid on
lim=min(find(isnan(RSD)==1))-10;
plot(positionmean(1:1:lim),RSD(1:1:li
m),'k','linewidth',2);
title('Relative Standard Deviation:
Case B - Injection nozzle 1');
xlabel('Piston position [mm]');
ylabel('RSD over 5 experiments');
axis([0 500 0 0.035]);
ax = gca;
ax.YTick = [0.005 0.010 0.015 0.02
0.025 0.03];

```

Datum  
 25.04.2018 13:01:54  
 Messreihe  
 EXB9nozZle2second  
 Pressure PT102  
 40,000000  
 Inverter speed  
 0,017300  
 Open Valve Time  
 7,430000  
 delay  
 0,000000

Encoder Position	open Valve	internal Pressure	internal Temperature	Temperature T135	I akt	time in ms	PT1NW1	in Bar	PT1NW2	in Bar	SV1NW1	SV1NW2
0,004487	0,000000	0,008692	108,649534	23,394839	0,017300	9041203,000000	4,857597	3,483273	25,369656	0,000000		
0,004494	0,000000	0,065037	108,649534	23,394839	0,017300	9041213,000000	6,438294	4,912195	25,369656	0,000000		
0,004489	0,000000	0,017912	108,649534	23,394839	0,017300	9041223,000000	9,374167	4,001949	25,369656	0,000000		
0,004466	0,000000	-0,006675	108,649534	23,394839	0,017300	9041233,000000	6,825780	3,434071	25,369656	0,000000		
0,004483	0,000000	0,004594	108,649534	23,394839	0,017300	9041243,000000	7,293224	5,568228	25,369656	0,000000		
0,004504	0,000000	0,066062	108,649534	23,394839	0,017300	9041254,000000	6,469047	3,784638	25,369656	0,000000		
0,004477	0,000000	0,015863	108,649534	23,394839	0,017300	9041264,000000	5,181527	6,086904	25,369656	0,000000		
0,004478	0,000000	0,024059	108,649534	23,394839	0,017300	9041285,000000	6,377584	5,391919	25,369656	0,000000		
0,004499	0,000000	-0,030238	108,649534	23,394839	0,017300	9041296,000000	5,687924	3,817440	25,369656	0,000000		
0,004502	0,000000	-0,025116	108,649534	23,388377	0,017300	9041306,000000	7,014398	4,844542	25,365281	0,000000		
0,004456	0,000000	0,046670	108,649534	23,388377	0,017300	9041316,000000	6,028256	4,088054	25,365281	0,000000		
0,004508	0,000000	0,046597	108,649534	23,388377	0,017300	9041326,000000	5,860140	3,647282	25,365281	0,000000		
0,004523	0,000000	0,013814	108,649534	23,388377	0,017300	9041336,000000	4,781740	5,152057	25,365281	0,000000		
0,004493	0,000000	0,073233	108,649534	23,388377	0,017300	9041346,000000	5,503407	3,616530	25,365281	0,000000		
0,004492	0,000000	-0,001553	108,649534	23,388377	0,017300	9041356,000000	7,902130	5,721986	25,365281	0,000000		
0,004507	0,000000	0,011765	108,649534	23,388377	0,017300	9041367,000000	8,787813	6,136107	25,365281	0,000000		
0,004489	0,000000	0,037377	108,649534	23,388377	0,017300	9041377,000000	6,784776	3,807190	25,365281	0,000000		
0,004489	0,000000	0,023034	108,649534	23,388377	0,017300	9041387,000000	5,415249	6,189409	25,365281	0,000000		
0,004524	0,000000	0,068111	108,649534	23,388377	0,017300	9041397,000000	4,642327	3,733386	25,365281	0,000000		
0,004544	1,000000	0,051719	108,649534	23,388377	0,017300	9041407,000000	6,624861	4,057302	25,365281	0,000000		
0,004499	1,000000	0,064013	108,649534	23,388377	0,017300	9041417,000000	6,026206	3,628831	25,365281	0,000000		
0,004531	1,000000	0,096796	108,649534	23,388377	0,017300	9041427,000000	6,524402	3,786689	25,365281	0,000000		
0,004559	1,000000	0,118309	108,649534	23,388377	0,017300	9041437,000000	4,992910	3,815390	25,365281	0,000000		
0,004526	1,000000	0,039426	108,649534	23,388377	0,017300	9041447,000000	5,212280	3,657532	25,365281	0,000000		
0,004534	1,000000	0,080404	108,649534	23,388377	0,017300	9041458,000000	5,109771	3,587829	25,365281	0,000000		
0,004519	1,000000	0,035328	108,649534	23,388377	0,017300	9041468,000000	2,432222	10,888045	25,365281	0,000000		
0,004574	1,000000	0,074257	108,649534	23,388377	0,017300	9041478,000000	2,612638	3,577578	25,365281	0,000000		
0,004577	1,000000	-0,030238	108,649534	23,388377	0,017300	9041489,000000	3,334306	7,909446	25,365281	0,000000		





*A conclusione di questo ciclo di studi e di questo lavoro di tesi, mi sembra doveroso porre i miei più sentiti ringraziamenti alle persone che ho avuto la fortuna di incontrare lungo il mio tragitto e che mi hanno aiutato a crescere sia dal punto di vista professionale che umano.*

*Un ringraziamento sentito va ad i miei relatori del Karlsruhe Institute of Technology, Evgenia Giakoumatou, Ann-Kathrin Goßmann, Björn Stelzner ed infine al Prof. Dimosthenis Trimis, senza il loro supporto e incoraggiamento per superare i numerosi momenti di difficoltà incontrati, questo lavoro non sarebbe stato possibile; ringrazio inoltre tutti i colleghi dell'Engler-Bunte-Institute per la calorosa accoglienza e l'aiuto ricevuto in questi mesi.*

*Un ringraziamento particolare va al Prof. Massimo Santarelli per il continuo supporto fornitomi a distanza dal Politecnico di Torino.*

*Ci tengo a ringraziare tutti i colleghi e amici conosciuti in questi anni, con i quali ho condiviso momenti davvero indimenticabili di gioia e di sconforto.*

*Ringrazio inoltre tutti gli amici di infanzia e di scuola che hanno sempre creduto in me e gli amici incontrati durante la mia esperienza Erasmus che mi hanno fatto sentire a casa sin da subito e dato la forza per portare a termine questo percorso.*

*Infine voglio ringraziare in modo speciale tutta la mia famiglia compresi i miei zii e chi non c'è più, per avermi insegnato a distinguere ciò che è giusto da ciò che è corrotto. Ringrazio ancora in modo particolare miei genitori per il continuo incoraggiamento e supporto datomi in questi anni, vorrei che questo mio traguardo, per quanto possibile, fosse un premio anche per i sacrifici che hanno fatto.*

**Antonio**